CHAPTER 6

Activity-based probes for retaining exo-mannosidases

Based on:

Kuo CL, Beenakker TJM, Lahav D, Hissink C, Armstrong Z, Wu L, Johnson R, de Boer C, Artola, M, Florea B, Boot RG, Codée JDC, van der Marel GA, Davies GJ, Aerts JMFG & Overkleeft HS. *To be submitted.*

ABSTRACT

Mannosidases are key enzymes in eukaryotic N-linked glycan synthesis and degradation. Among these hydrolases, retaining exo-α-mannosidases (Glycoside Hydrolase (GH) family 38) and exo-β-mannosidase (GH family 2) are implicated in pathologies such as cancer and lysosomal storage diseases. To generate tools to profile these enzymes, mechanism-based suicide inhibitors and activity-based probes (ABPs) were synthesized and characterized. These compounds, based on α-mannose or β-mannose configured cyclophellitol scaffolds, are micromolar inactivators of their expected target enzymes. The ABPs label the target mannosidases in mechanism-based manner, as confirmed by SDS-PAGE-based fluorescent detection, kinetic studies, and protein crystallography. Proteomics revealed that the α-mannose configured ABP equipped with biotin labels all five GH38 retaining exo-α-mannosidases in mouse tissue extracts. Similarly, the α-mannose configured Cy5 ABP labels all five human GH38 α-mannosidases cloned and individually expressed in human cell lines. The unique molecular weight and pH optimum of each α-mannosidase allows their simultaneous activity-based profiling in complex biological samples such as cell lysates and tissue extracts. β-Mannose configured ABP labels the GH2 β-mannosidase (MANBA) in mouse kidney extracts. It additional labels retaining β-glucosidases, but specific visualization of MANBA is still feasible by pre-incubating the samples with β-glucosidase inhibitors. In conclusion, the novel ABPs described here enable the simultaneous visualization of all retaining exo-mannosidases in complex biological samples. They should assist future screening for small molecule inhibitors/activators of these highly relevant enzymes.

6.1 Introduction

Protein N-linked glycosylation takes place in all domains of life. In the ER of eukaryotes, it plays essential roles in folding ,quality control and subsequent transport of newly formed N-linked glycoproteins to the Golgi apparatus.[1, 2] This finely orchestrated process is carried out by lectins recognizing specific glycan structures, and by glycosidases residing at various subcellular locations that modify the glycans. A key component of the N-linked glycan is mannose. This sugar is abundant in the $Glc_3Man_9GlcNAc_2$ glycan that is transferred from the dolichol donor to nascent polypeptide in the ER (**Fig. 6.1**, step 1−2). Maturation of N-linked glycoprotein is accompanied by removal of specific mannose residues from their N-linked glycans. Several mannosidases are involved in this process. These enzymes differ in subcellular location and substrate specificity, and are classified into Glycoside Hydrolase (GH) family 2, 38, 47, and 99 (**Fig. 6.1**, bottom right) based on the Carbohydrate active enzyme (CAZy) database[3].

In man, the GH47 family comprises four inverting exo-α-1,2-mannosidases located in the ER and Golgi complex, and three additional ER-dependent α-mannosidase-like proteins (EDEMs) that have putative α-mannosidase activity. The ER-α-mannosidase I (MAN1B1) trims one mannose from the protein N-linked glycan, which signals the protein to either pass the ER quality control checkpoint (**Fig. 6.1**, step 3−4)[4, 5] or enter the ER-associated degradation pathway in a process facilitated by the EDEMs (**Fig. 6.1**, step 5−6).[6, 7] The three Golgi GH47 mannosidases, Ia (MAN1A1)[8], Ib (MAN1A2)[9], and Ic (MAN1C1)[10] further trim the α-1,2-linked mannoses from glycans of glycoproteins arriving at the *cis*-Golgi (**Fig. 6.1**, step 7−8), enabling downstream processes such as protein N-linked hybrid- or complex-type glycan synthesis (**Fig. 6.1**, step 11−12 and below) or the mannose-6-phosphate mediated endosomal/lysosomal targeting (**Fig. 6.1**, step 13 and below)[11]. The GH99 endo-α-1,2-mannosidase (MANEA) is also residing at the *cis*-Golgi. It recognizes glycoproteins that still contain terminal glucose residues and catalyzes the one-step endo-glycosidic hydrolysis of these glucoses together with the adjacent mannose. This provides an additional pathway for glycoprotein maturation (**Fig. 6.1**, step 9−10).[12, 13]

The other two mannosidase families are GH38 α-mannosidase (MAN2A1, MAN2A2, MAN2B1, MAN2B2, MAN2C1) and GH2 β-mannosidase (MANBA), both composed of

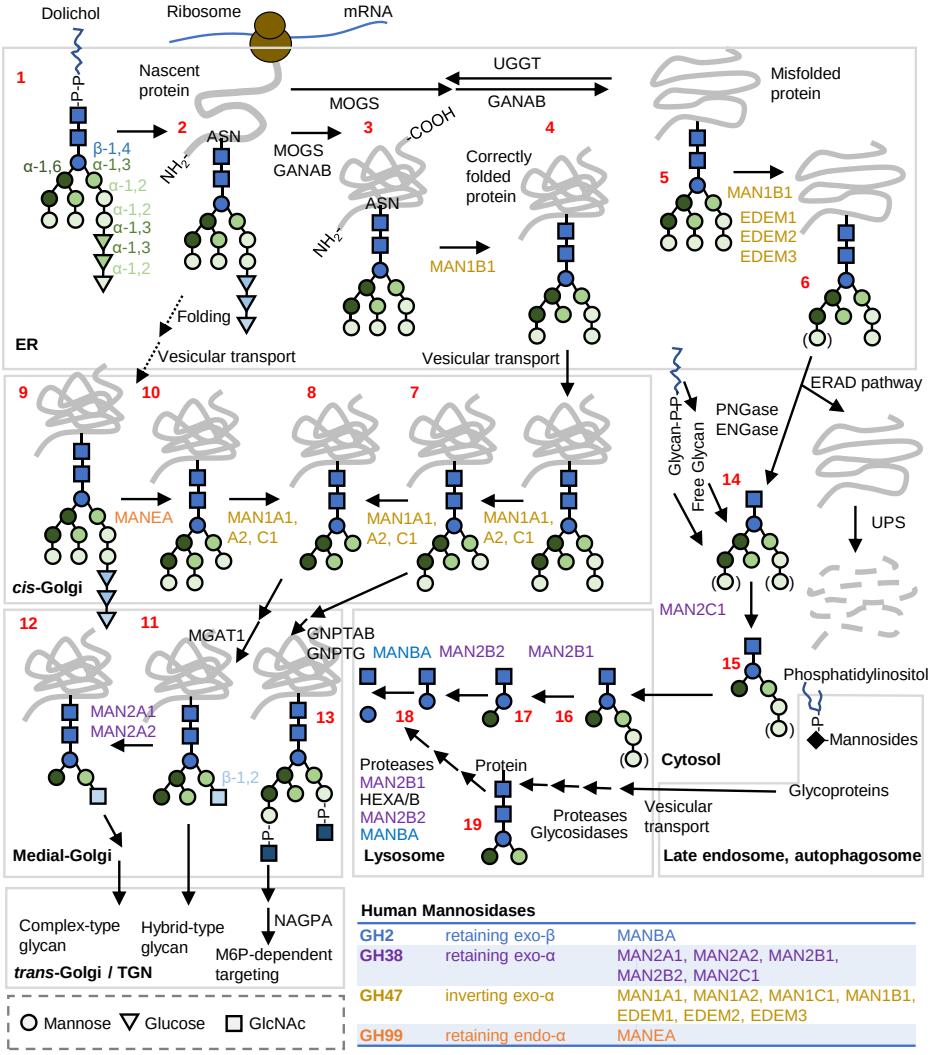

Figure 6.1. Human mannosidases in N-linked glycoprotein synthetic and degradation pathways. 1−4, trimming of glucoses and one mannose on correctly folded proteins in the ER. 5−6, mannosidases responsible for initiating the ER-associated degradation (ERAD) pathway. 7−8, mannose trimming in the *cis*-Golgi. 9−10, action of the endo-mannosidase on glycoproteins arriving at the Golgi with terminal glucoses. 11−12, mannose trimming by Golgi mannosidase II and IIx (MAN2A1, A2) for complex-type glycan formation. 13, glycan processing for the mannose-6-phophate (M6P)-dependent protein targeting pathways. 14−15, glycan degradation by cytosolic mannosidase (MAN2C1). 16−19, actions of lysosomal retaining exo-mannosidases (MAN2B1, B2, and MANBA) on glycans from the cytosol or endosomal compartments. *UPS*, ubiquitin-proteasome system; *MOGS*, ER α-glucosidase I; *GANAB*, ER α-glucosidase II; *UGGT*, UDP-glucose:glycoprotein glucosyltransferase; *GNPTAB/GNPTG*, GlcNAc-phosphotransferase α, β/γ subunits; *NAGPA*, GlcNAc1-1-phosphodiesterase; *MGAT1*, α-1,3-mannosyl-glycoprotein 2-β-GlcNAc transferase.

retaining glycosidases. The human GH38 α-mannosidase family consists of five members, all of which require metal ions (zinc or cobalt) for catalysis but differ in subcellular location and substrate specificity. Two of these, Golgi mannosidase II[14] and IIx[15] (MAN2A1 and MAN2A2, E.C. 3.2.1.114), remove the two outer α-1,3- and α-1,6-linked mannoses on the protein $GlcNAcMan_4GlcNAc_2$ glycans, thus allowing further synthesis of complex-type glycans (**Fig. 6.1**, step 11−12).[16] These two enzymes arose from a recent mammalian gene duplication event, exhibiting overlapping substrate specificity[17] but differ in expression levels depending on tissue type.[18, 19] The neutral α-mannosidase (MAN2C1) is a cytosolic enzyme degrading soluble N-linked glycans released from glycoprotein or glycolipids into $Man_5GlcNac$, thus allows the trimmed glycan to be further degraded in the lysosome (**Fig. 6.1**, step 14−15).[20, 21] It depends on Co^{2+} for catalysis, but is also activated by Fe^{2+} and Mn^{2+}.[22] The lysosomal GH38 α-mannosidase MAN2B1 acts on α-1,2- and α-1,3-linked mannoses on glycans derived from protein N-linked glycans or glycolipids (E.C.3.2.1.24),[23] as well as on glycans attached to glycoproteins (**Fig. 6.1**, step 16 and 19).[24] It does not cleave the core α-1,6-linked mannose,[24] which is specifically hydrolyzed by the lysosomal GH38 core-specific α-mannosidase (MAN2B2, E.C. 3.2.1.114) (**Fig. 6.1**, step 17 and 19),[25, 26] also known as the epididymis α-mannosidase.[27] Finally, the lysosomal GH2 β-mannosidase (MANBA) releases the last mannose residue from GlcNAc (E.C. 3.2.1.25) and completes the mannose catabolism (**Fig. 6.1**, step 18 and 19).[28, 29]

Both the GH38 and GH2 mannosidases receive continuous interest as therapeutic targets for human diseases. The Golgi α-mannosidase MAN2A1 has been linked to the progression of several cancers.[30] Clinical trials had been conducted using the inhibitor swainsonine, albeit unsuccessful due to adverse side effects attributed to its concomitant inhibition of other mannosidases [31, 32] Inherited deficiency of the lysosomal α-mannosidase MAN2B1 deficiency underlies the lysosomal storage disorder α-mannosidosis (OMIM: 248500) in man.[33] Affected individuals accumulate in lysosomes undegraded mannose-containing oligosaccharides, causing variable degree and progression of mental and respirational impairment, hearing loss, Hurler-like facial distortion, and reoccurring infections among paitents.[33] A recombinant α-mannosidase-based enzyme replacement therapy has been recently approved in the EU.[34, 35] Deficiency in the lysosomal β-mannosidase MANBA also causes a lysosomal storage disorder, β-mannosidosis (OMIM: 248510). This disease is firstly described in goat[36] and is rare in human. Human patients generally have milder symptoms (e.g. mental retardation) compared to the affected lifestock.[37] Last but not least, the cytosolic neutral α-mannosidase MAN2C1 is

involved in tumorigenesis.[38, 39] The cause for this process is believed to be independent of MAN2C1's catalytic activity, but rather through its direct association with tumor suppressive proteins and thereby causes their inactivation during tumorigenesis.[40, 41]

In the past, GH38 α-mannosidase activities are distinguished from those of GH47 α-mannosidases based on their different cation preference (Zn^{2+} or Co^{2+} for GH38 *vs* Ca^{2+} for GH47) and inhibitor sensitivity (furanose-based inhibitors such as swainsonine and mannostatin A for GH38; pyranose-based inhibitors such as 1-deoxymannojirimycin for GH47).[42] Because GH38 and GH2 mannosidases are retaining glycosidases employing the Koshland double displacement catalytic mechanism (**Fig. 6.2A, B**),[43−45] it is envisioned that their activity can be selectively measured over the GH47 enzymes (which are inverting glycosidases) by activity-based protein profiling with compounds harboring a mannose-configured scaffold that covalently becomes trapped at the catalytic nucleophile of the enzyme upon the initial nucleophilic attack (**Fig. 6.2C, D**). Similar approaches using configurational isomers of cyclophellitols and cyclophellitol aziridines have been recently demonstrated to be useful tools in labeling their targeted glycosidases (General Introduction and Chapter 6, this thesis). This chapter presents the characterization of the α- or β-mannose configured cyclophellitol aziridines inhibitors and ABPs in their inhibitory potency and labeling towards GH38 and GH2 mannosidases, and discusses the potential application of the ABPs in the study of mannosidase biology and associated diseases.

6.2 Results

6.2.1 Synthesis of compounds used in this chapter

The synthesis of compounds **1**−**7** and **8**−**13** was performed at the Department of Bio-organic Synthesis at Leiden University and followed the strategies reported for the α- and β-mannose configured cyclophellitols **1** and **8**,[46] the β-mannose configured cyclophellitol aziridine **9**,[46] and the α-mannose configured cyclophellitol aziridine **2**[47] (**Fig. 6.3** and **Scheme 6.S1**−**2**). N-alkylation of **2** or **9** with 1-azido-8-iodooctane yielded compound **3** and **10**, which were subsequently appended with either a BODIPY, Cy5, or a biotin tag (compounds **4**−**6** and **11**−**13**) using the Cu(I)-catalyzed azide-alkyne Huisgen [2 + 3]-cycloaddition ("click" reaction).[48, 49] N-acylation of **3** was also attempted,[48] with which successfully yielded the Cy5 compound **7**.

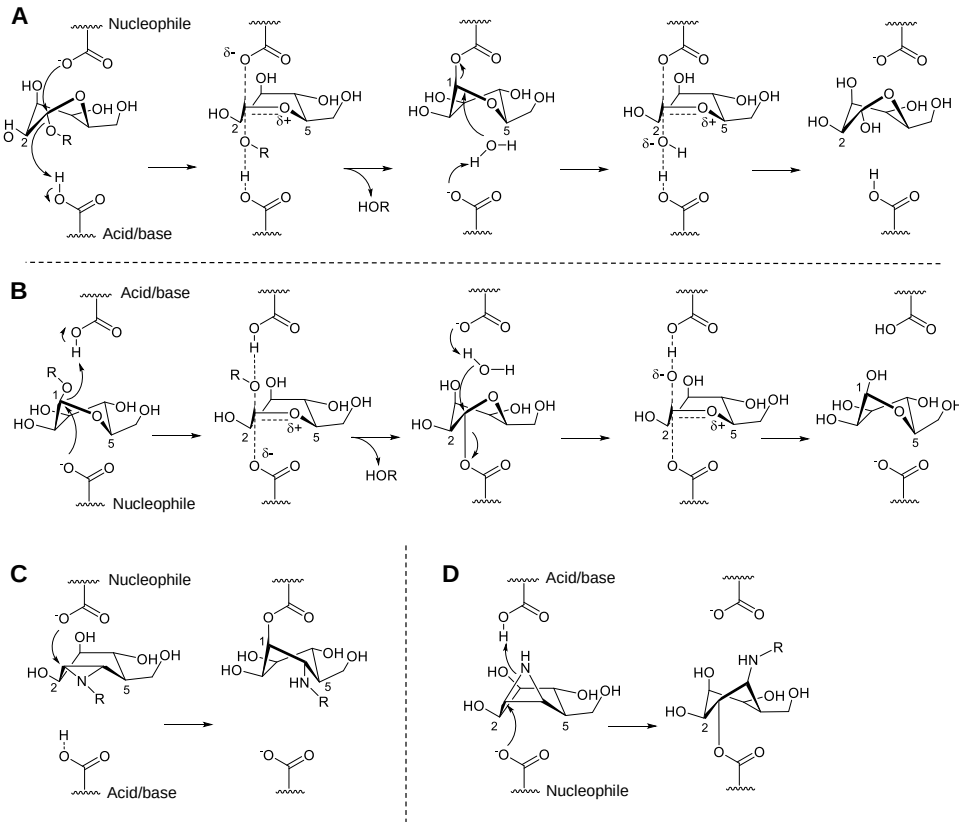

Figure 6.2. Reaction mechanisms of retaining exo-mannosidases. A) Reaction itinerary by GH38 α-mannosidases. B) Reaction itinerary by GH382 β-mannosidase. C) Proposed reaction mechanism for α-mannose configured cyclophellitol aziridine. D) Proposed reaction mechanism for β-mannose configured cyclophellitol aziridine. Numbers shown correspond to pyranose numbering of the carbons.

6.2.2 *In vitro* activity of compound **1**−**7** on GH38 α-mannosidases

The α-mannose configured compounds **1**−**7** were tested for *in vitro* inhibitory potency by enzymatic assay of commercially available Jack bean (*Canavalia ensiformis*) GH38 α-mannosidase (E.C. 3.2.1.24). This enzyme exhibits a similar catalytic profile and zinc ion dependency to the human lysosomal broad-specificity α-mannosidase (MAN2B1).[50] The assay was performed at an acidic pH of 4.5 and at 37 °C, by means of a 30 min incubation of enzyme with compounds and the substrate, 4-methylumbelliferyl-α-D-mannopyranoside (4-MU-α-man).

It turned out that all the tested compounds were α-mannosidase inhibitors, exhibiting low- to mid-micromolar apparent IC_{50} values (**Table 6.1**, **Fig. 6.S1A**). The most potent of the series were the biotin **6**, Cy5 **5**, and N-alkyl azide compound **3** (apparent IC_{50} = 2−4 μM); they were followed by the unsubstituted α-mannose configured cyclophellitol aziridine **2**, and the epoxide **1**, with the later having similar value to the one reported by Tatsuta et al.[51] BODIPY ABP **4** was the least potent of the series, having apparent IC_{50} value over 50 μM. The N-acylated Cy5 ABP **7** required more steps to synthesize but was equally potent as the N-alkylated Cy5 ABP **5**, similar

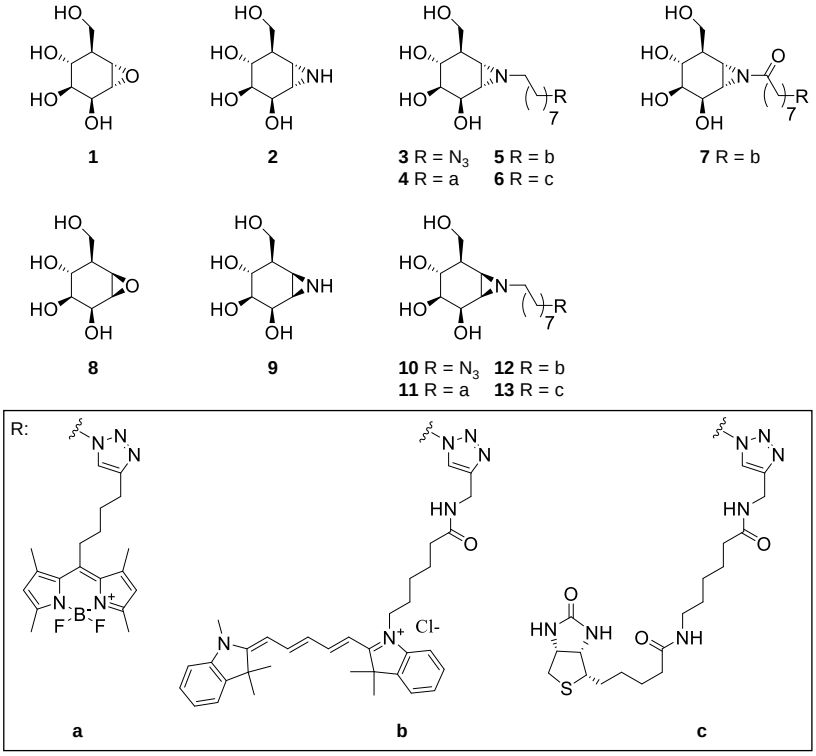

Figure 6.3. Structures of compounds used in this study.

Table 6.1 Apparent IC_{50} values of α-mannose configured cyclophellitol and aziridines towards Jack bean GH38 α-mannosidase. A) Apparent IC_{50} values at 30 min compound incubation time. B) Apparent IC_{50} values of **5** at different incubation time.

A

Compounds	IC_{50} (μM)
1 (TB440)	35.4 ± 6.70
2 (TB450)	7.19 ± 0.12
3 (TB481)	3.54 ± 0.48
4 (TB521)	> 50
5 (TB482)	3.43 ± 0.68
6 (TB484)	2.22 ± 0.24
7 (TB480)	3.86 ± 1.30

B

Incubation time (min)	IC_{50} (μM)
10	4.94 ± 0.13
30	2.84 ± 0.17
120	1.13 ± 0.06

to the general trend observed on earlier reported ABPs towards other glycosidases.[52] Next, time dependency of inhibition by ABP **5** was examined. The apparent IC_{50} values for the N-alkyl ABP **5** gradually were found to decrease from 4.94 μM to 1.13 μM with incubation times increasing from 10 min to 120 min (**Table 6.1B, Fig. 6.S1B**), hinting to irreversible inhibition.

Next, SDS-PAGE-based fluorescent readout was used to directly visualize the covalent ABP labeling of Jack bean α-mannosidase. In the first experiment, 3 μM ABP **5** was incubated with the enzyme for 30 min at 37 °C at various pHs. The results showed that the ABP covalently labeled the enzyme in a pH-dependent manner: one band between 60 and 70 kDa was found to be most prominently labeled at acidic pHs (**Fig. 6.4A**, left), corresponding to the known size of the large subunit (66 kDa) of Jack bean α-mannosidase bearing the active site.[51] Removing zinc ion from the reaction mixture did not affect the ABP labeling during the 30 min incubation time (**Fig. 6.4A**, left). Compared to enzymatic activity, the ABP labeling had a slight shift in pH optimum (0.5−1 unit)—with maximal enzymatic activity occurring at pH 4.5−5.0 and maximal ABP labeling at pH 5.0−6.0 (**Fig. 6.4A**, right). The labeling potency of ABP **5** was next compared to that of ABP **7** (N-acyl Cy5) at pH 5.5: both labeled the enzyme and were equally potent (**Fig. 6.4B**). Saturation of labeling occurred at around 3 μM for both ABPs, with the calculated concentration for 50 % labeling being 0.3 μM (**Fig. 6.4B**, right). This value was ten-fold lower than the apparent IC_{50} values (around 3 μM), which might be resulted from different assay pHs (5.5 during ABP labeling *vs* 4.5 during inhibitory IC_{50} determination). Time-dependency of labeling by ABP **5** was next examined, at 3 μM ABP **5** and pH 5.5. It was found

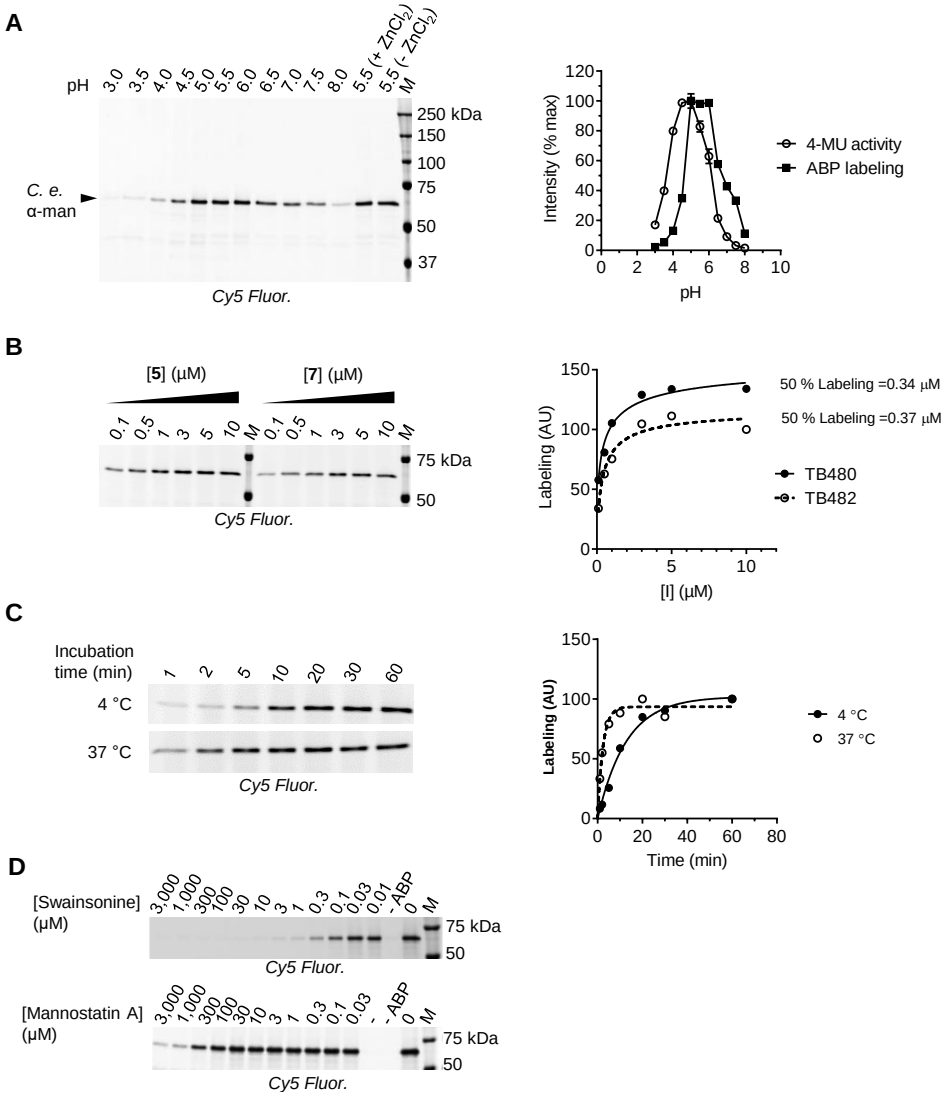

Figure 6.4. *In vitro* labeling of compounds towards Jack bean (*Canavalia ensiformis*) GH38 α-mannosidase. A) pH-dependent labeling of **5** (left) and comparison of quantified ABP labeling with measured 4-MU activity across different pHs. Error ranges = ± SD from technical triplicates. B) Labeling of **5** and **7** at different ABP concentrations (left) and band quantification (right). C) Time-dependent labeling of **5** at two different temperatures (left) and band quantification (right). D) Competitive ABP labeling of **5** against pre-incubation of swainsonine and mannostatin A. -, empty lane.

that labeling increased with incubation time, and reached saturation within 10 min at 37 °C (60 min for labeling at 4 °C) (**Fig. 6.4C**). Finally, to determine if the labeling occurred at the enzymes' active site pocket, the enzyme was pre-incubated with two known GH38 α-mannosidase inhibitors, swainsonine and mannostatin A, followed by a short ABP labeling period of 10 min. As expected, labeling of ABP **5** towards the enzyme was abolished by both inhibitors, suggesting active-site pocket occupancy of the ABPs in the enzyme (**Fig. 6.4D**).

The active site occupancy and labeling of the compound towards GH38 α-mannosidase was further examined in detail by structural analysis perform at the University of York. For this experiment, protein crystals of the *Drosophila melanogaster* GH38 MAN2A1 (Golgi α-mannosidaseII) homologue (dGMII)[30] were incubated with the bare aziridine compound **2**, and solved for structure by protein X-ray crystallography. In the resolved structure, a covalent glycosidic bond was clearly visible between the C1 of compound **2** and the catalytic nucleophile Asp204 (**Fig. 6.5**) of dGMII. Compound **2** adopted an $^{1}S_{5}$, conformation (**Fig. 6.5**, right), matching the known substrate conformation at the covalent enzyme-substrate intermediate (**Fig. 6.2A**, middle).[45]

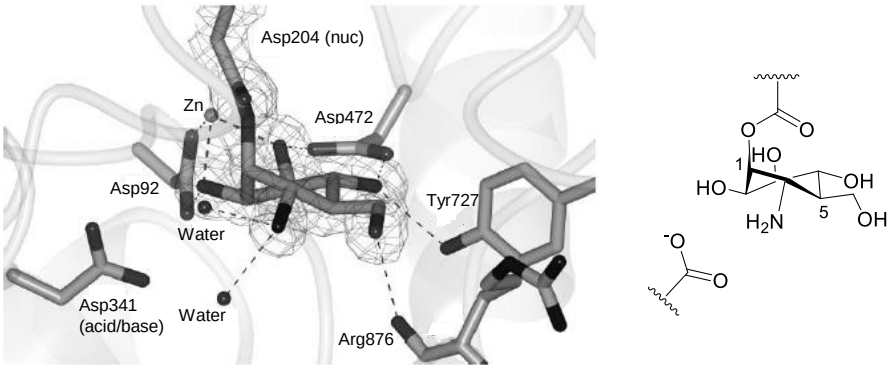

Figure 6.5. Structure of *Drosophila melanogaster* GH38 α-mannosidase (dGMII) in complex with compound 2. Right, skeletal structure of compound **2** bound to the nucleophile, showing the conformation observed from the crystal structure (left).

6.2.3 Target detection and identification of the α-mannose configured ABPs in complex biological samples

Activity-based protein profiling (ABPP) was performed with ABP **5** in mouse tissue extracts. Titration of ABP concentration from 0.03 to 10 μM at pH 5.5 in homogenates of liver,

spleen, kidney, and testis enabled the detection of distinct bands in these samples. At 1−3 μM ABP **5**, a sharp band around 140 kDa was detected in liver and testis extracts, whilst two bands around 50 kDa and 45 kDa were clearly visible in spleen, kidney, and testis extracts (**Fig. 6.6A**). As testis extracts contain multiple bands, a pH titration was performed herewith from pH 3.0 to 8.0. The experiment revealed that the labeling of the different bands had a distinct pH optimum; the 140 kDa band was optimally labeled at pH 6.0, while the 50 and 45 kDa bands were optimally labeled at pH 4.5 (**Fig. 6.6B**). Several other minor bands were also detected, most of which also showed a pH optimum of 4.5. To determine whether these bands were GH38 α-mannosidases, a competitive ABPP (cABPP) experiment was employed. Mouse testis extracts were pre-incubated with swainsonine or mannostatin A for 30 min at pH 4.5, and then incubated with 3 μM ABP **5** for 10 min. The 140 kDa, 50 kDa, 45 kDa, and an additional 76 kDa bands were abolished by swainsonine pre-incubation, and the 45 kDa band was additionally competed away

Figure 6.6. ABPP in mouse tissue extracts with ABP 5. A) Concentration titration of ABP **5** in

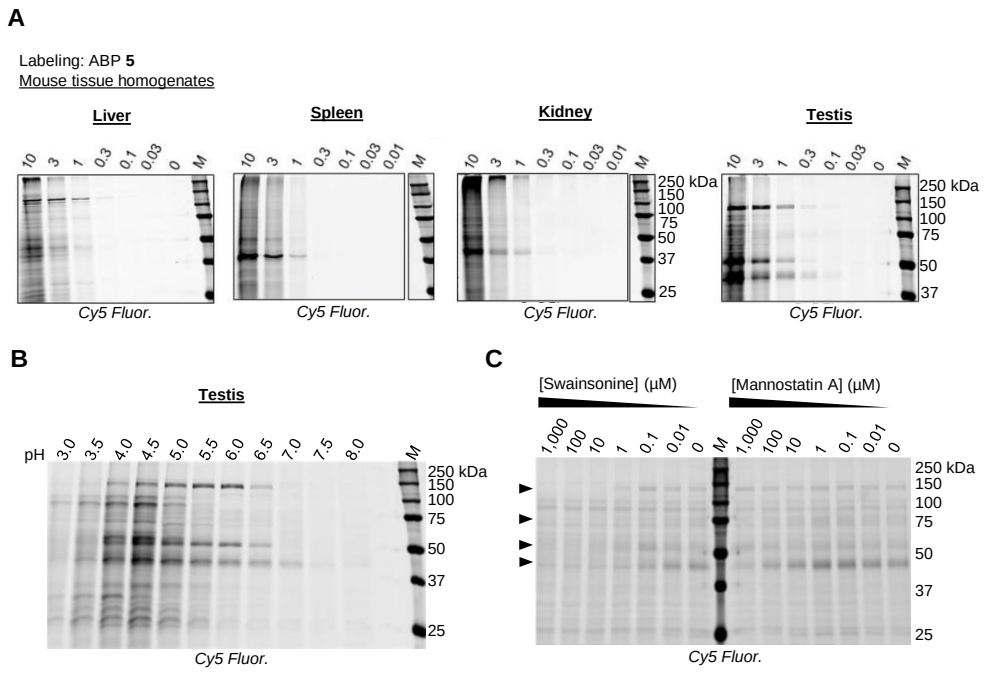

homogenates of liver, spleen, kidney, and testis. B) Titration of labeling pH with ABP **5** in mouse testis homogenates. C) cABPP of swainsonine or mannostatin A with ABP **5** in mouse testis homogenates. Arrows, bands that were abolished by swainsonine pre-incubation.

with 1 mM mannostatin A (**Fig. 6.6C**). The other minor bands were not abolished by inhibitor

pre-incubation, pointing to non-specific labeling (**Fig. 6.6C**). MANB1 is cleaved in the lysosome into five fragments that contain the 42 kDa peptide A (with catalytic active site), the 10 kDa peptide B, the 24 kDa peptide C, and peptide D and E; the latter two do not form disulfide bridges to the other three fragments.[23, 32] Thus, the 76, 50, and 45 kDa bands, all showing a labeling pH optimum of 4.5, could correspond to MAN2B1's peptide ABC, AB, and A, respectively. The 140 kDa with a labeling pH optimum of 6.0 and being abolished by swainsonine pre-incubation is likely MAN2A1 and/or A2.

A parallel experiment using the biotin ABP **6** was performed in mouse testis extracts to verify the labeling of GH38 enzymes. Samples incubated with ABP 6 at either pH 4.5 or 6.0 were subjected to biotin affinity enrichment and tryptic digestion (both on-bead digestion and in-gel digestion), and finally LC-MS-based protein identification. While silver stain of the gel containing the affinity-enriched samples yielded few, if any, distinct bands (data not shown), the on-bead digest protocol identified MAN2B1 and MAN2B2 in the sample labeled by ABP **6** at pH 4.5, and all five GH38 α-mannosidases in the sample labeled at pH 6.0 (**Table 6.2**). No other glycosidases were detected in these samples.

Table 6.2. List of identified glycosidases by LC-MS-based proteomics in samples of mouse testis extracts incubated with ABP 6. PLGS, ProteinLynx Global Server.

Condition	Accession	Entry	PLGS Score	Peptides	Theoretical peptides	Coverage (%)
pH 4.5	O09159	MAN2B1_MOUSE	175	9	64	9
	O54782	MAN2B2_MOUSE	306	28	57	20
pH 6.0	P27046	MAN2A1_MOUSE	391	28	84	22
	Q8BRK9	MAN2A2_MOUSE	63	6	78	6
	O09159	MAN2B1_MOUSE	175	6	64	9
	O54782	MAN2B2_MOUSE	306	16	57	16
	Q91W89	MAN2C1_MOUSE	119	12	63	14

To shed definitive light on the labeled mannosidases, in a final experiment all five human GH38 α-mannosidases were individually cloned and expressed in HEK293T cells, and the cell lysates were labeled at various pHs with ABP **5**. Lysates of cells transfected with MAN2A1 and MAN2A2 shown bands at around 140 kDa and labeled optimally at pH 5.5−6.0 (**Fig. 6.7**). Lysates of cells transfected with MAN2B1 showed multiple bands optimally labeled

at pH 4.0−5.5, with molecular weights of 130 kDa, 65 kDa, 45 kDa, and 30 kDa. This labeling pattern possibly reflects the complex processing and maturation of MAN2B1 in the lysosome (**Fig. 6.7**). Lysates of cells transfected with MAN2B2 showed a weaker 130 kDa band and a prominent 50 kDa band, both of which had pH optimum around 4.0−5.5 (**Fig. 6.7**). Lysates of cells transfected with MAN2C1 showed a band just above 100 kDa and most prominently at pH 6.5. It is also prominently labeled at pH 7.5, which is different from other GH38 enzymes expressed in HEK293T cells (**Fig. 6.7**).

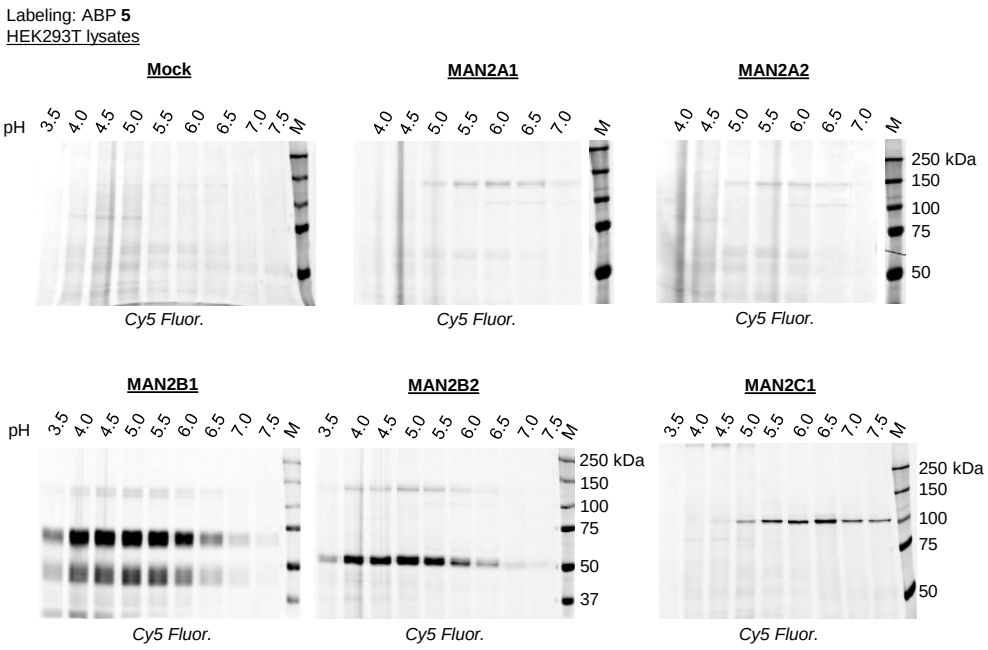

Figure 6.7. ABPP in lysates of HEK293T cells transfected with human GH38 α-mannosidases.

While it was not possible to discriminate MAN2A1 from MAN2A2 in the ABPP setup due to their similar pH range and molecular weight, the other four enzymes were readily identifiable by ABP labeling at different pH values. It was observed that MAN2A1/A2 were most prominently expressed in mouse testis and less in HEK203T cells and mouse brain and epididymis; MAN2B1 and MAN2B2 were expressed in all the samples, whilst MAN2C1 was only observed in mouse brain (**Fig. 6.8**). In mouse epididymis extracts, the 65 kDa and 45 kDa

MAN2B1 seemed to have multiple forms that differ in molecular weights, in contrast to the sharp bands observed in mouse brain extracts.

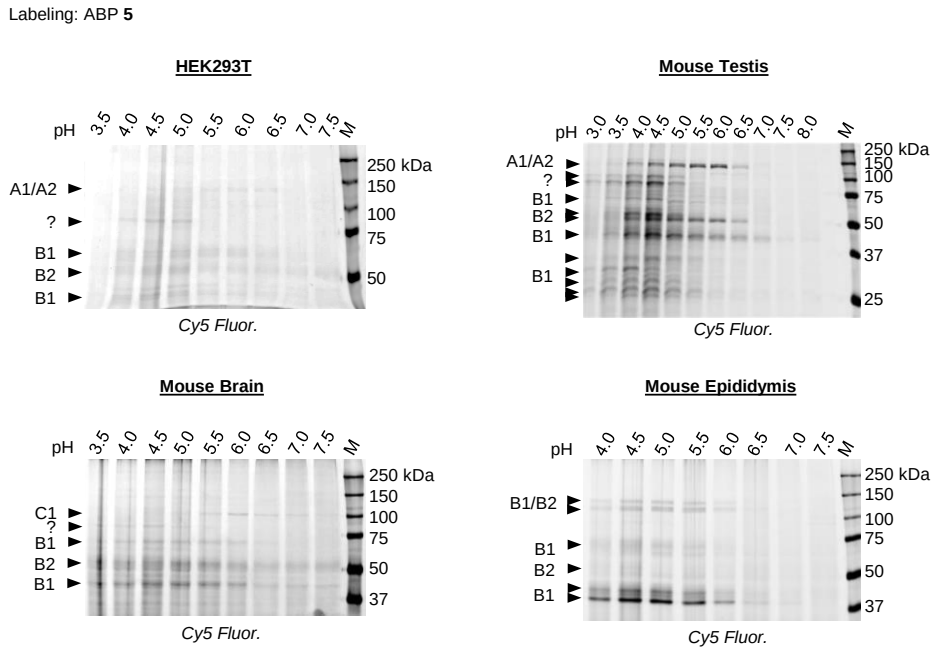

Figure 6.8. Assigning GH38 α-mannosidases in cell lysates and tissue extracts labeled with ABP 5.

6.2.4 *In vitro* activity of compound **8**−**13** towards GH2 β-mannosidase

Next, the β-mannose configured compounds were characterized regarding inhibitory potency and labeling characteristics using commercially available GH2 β-mannosidase from Roman snail (*Helix pomatia*).[54] Initial apparent IC_{50} measurements were performed by means of 30 min incubation of enzyme with compounds and the substrate 4-MU-β-D-(4-MU-β-Man) at pH 4.2, the optimum pH for the enzyme.[55] However, none of the compounds inhibited the enzyme, even at the highest concentration (50 μM). To verify this observation, labeling at various pH values was examined. In this experiment, 10 μM of the Cy5 ABP **12** was incubated with the enzyme for 1 h across a range of pH from 3.0 to 7.0 in the presence of bovine serum albumin (BSA, which stabilized the enzyme at pH > 3.5 (**Fig. 6.S3A, B**)), and samples were subjected to SDS-PAGE-based fluorescence detection. It turned out that a prominent band was detected

from pH 4.0 to 7.0 at just below 100 kDa (**Fig. 6.9A**, left, **Fig. 6.S3C**), which matched the known molecular weight (94 kDa) of the snail GH2 enzyme.[54] Band quantification showed that optimum labeling occurred at pH 5.5, and the labeling decreased rapidly at higher and lower pH (**Fig. 6.9A**, right, red). Similar to the α-mannose configured Cy5 ABP **5**, the relative ABP labeling

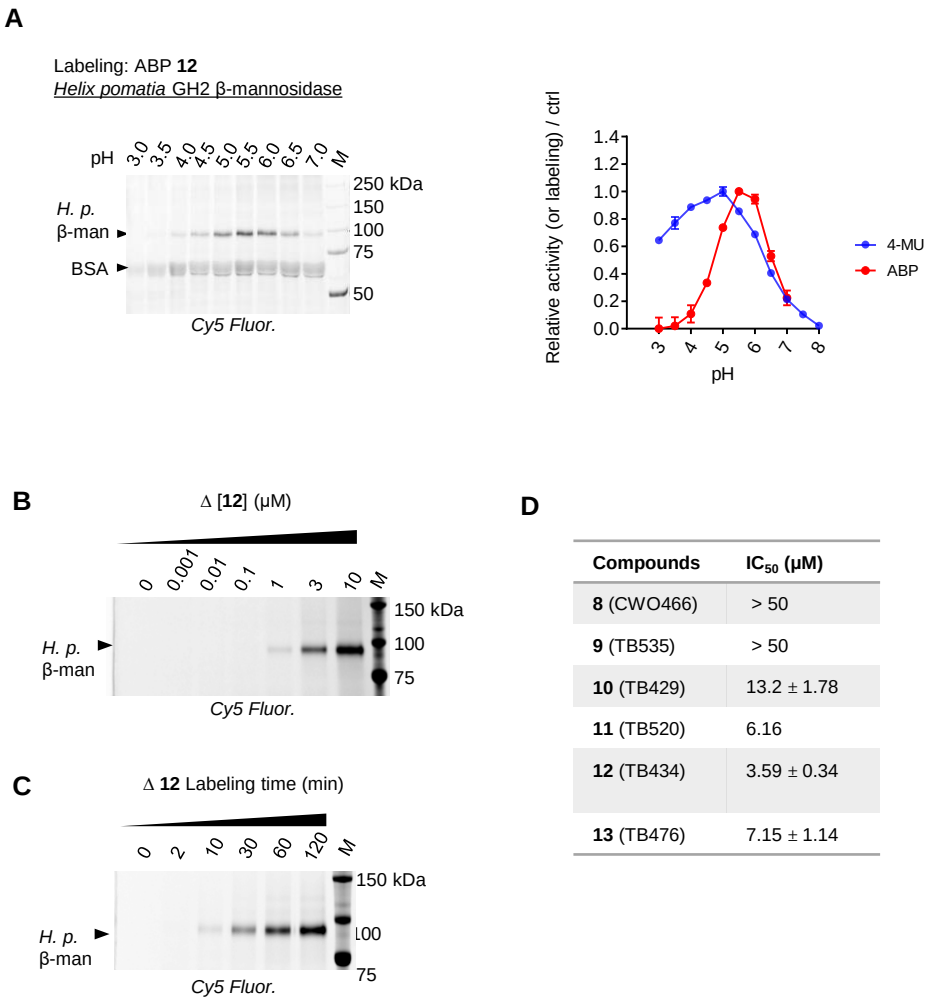

Compounds	IC_{50} (μM)
8 (CWO466)	> 50
9 (TB535)	> 50
10 (TB429)	13.2 ± 1.78
11 (TB520)	6.16
12 (TB434)	3.59 ± 0.34
13 (TB476)	7.15 ± 1.14

Figure 6.9. Labeling and inhibitory potency of compounds towards GH2 β-mannosidase from Roman snail (*Helix pomatia*). A) ABP **12** labeling at various pHs (left) and comparison of the quantified band intensity with relative enzymatic activity across pHs (right). B) Labeling of ABP **12** at various ABP concentration. C) Labeling of ABP **12** at various incubation time. D) Apparent IC_{50} values of compounds **8**–**13**.

intensity was lower than the enzymatic activity at acidic pH. This effect was not due to the instability of the ABP at acidic pH, as labeling with ABPs pre-incubated at different pH values over a period of 0–60 min showed identical intensity (**Fig. 6.S3D**). At pH higher than 5.5, the relative labeling by ABP **12** generally matched the enzymatic activity.

Using the determined optimal labeling pH (5.5), ABP **12** was next incubated with the β-mannosidase at various ABP concentration and labeling time. Labeling increased with both ABP concentration and labeling time, and saturate labeling in the experiments was observed at 10 μM ABP (1 h incubation) (**Fig. 6.9B**) and 120 min incubation (10 μM ABP) (**Fig. 6.9C**). Using these conditions (pH 5.5, 2 h incubation), IC_{50} measurement was performed again for all the β-mannose configured compounds. The results showed that at these reaction conditions, the compounds did inhibit the enzyme's hydrolysis of 4-MU-β-man (**Fig. 6.9D**). ABP **12** was the most potent of the series (apparent IC_{50} = 3.6 μM), followed by the BODIPY ABP **11**, the biotin ABP **13**, and the alkyl azide **10**. The bare epoxide **8** and aziridine **9** turned out not to inhibit the enzyme at the highest compound concentration tested (50 μM) (**Fig. 6.S3**).

6.2.3 Kinetic parameters determination for ABP **12** towards GH2 β-mannosidase

In previous chapters, a continuous method (simultaneous incubation of inhibitor and fluorogenic substrate) has been utilized for assessing the kinetic parameters of the β-glucuronidase ABP towards its target enzyme (Chapter 4, this thesis). However, due to its high potency and fast binding kinetics, only the pseudo-first order kinetic parameter (k_{inact}/K_I) could be obtained (Chapter 4, this thesis). A gel-based method has also been employed for the determination of kinetic parameters K_I (inhibition constant) and k_{inact} (inactivation rate constant) for the slower-reacting α-iduronidase ABP (Chapter 5, this thesis). While it completely circumvented the influence of added substrates, it was more laborious than the fluorogenic substrate assay. An alternative approach was used here, in which free ABP in the reaction mixture was removed by chromatography spin column, before the samples were added with 4-MU substrates and measured for fluorescence in 96-well plates. The extra step in removing free ABPs before adding substrates should theoretically prevent any influence from the substrates during ABP labeling, making the determination of kinetic parameters more accurate.

To verify this approach in free ABP removal, the snail GH2 enzyme was firstly labeled with 10 μM ABP **12** for 2 h at pH 5.5, and subjected to polyacrylamide desalting spin column

for two times. The extent of removal of unbound ABPs was checked by SDS-PAGE-based fluorescence detection. The gel showed that the unbound ABPs, which were migrated to the bottom of the gel, were mostly removed after consecutive spin column (**Fig. 6.10A**). Interestingly, the first spin column removed 98.5 % of the unbound ABPs in the samples, while the second column only removed less than half of the remaining unbound ABPs (**Fig. 6.10A**, right). The enzyme amount was partially affected by the spin columns, but a yield of 73 % was still obtained after the consecutive columns (**Fig. 6.S4**). With the method in place, the enzyme was next

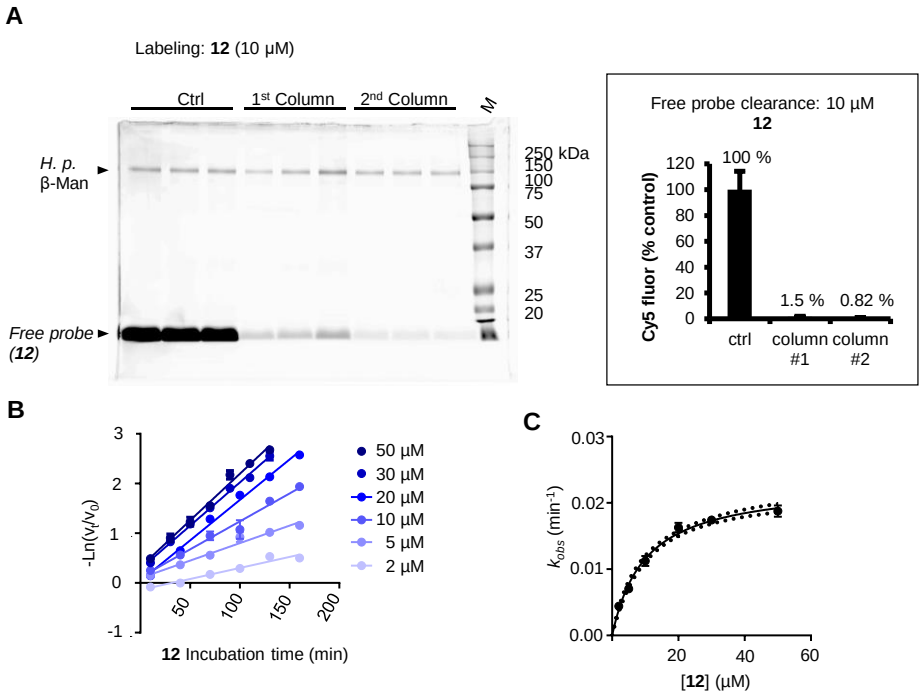

D

Compound	K_i (µM)	k_{inact} (min^{-1})	k_{inact}/K_i ($\mu M^{-1}min^{-1}$)
12	9.92 ± 0.94	0.023 ± 0.001	0.0023

Figure 6.10. Determination of inhibitory kinetics of ABP 12 towards *Helix pomatia* GH2 β-mannosidase. A) Assessing free-probe clearance by consecutive desalting columns using SDS-PAGE-based fluorescence scanning (left); quantified relative band intensity from the free probe (right). Error ranges = SD from *n* = 2 experiments. B) Inverted logarithmic plot of relative enzymatic reaction rate of various ABP concentration at different incubation time C) Michaelis-Menten plot of the derived k_{obs} at various ABP concentration. D) Derived kinetic parameters. Error ranges = SD from *n* = 3 experiments.

incubated with ABP **12** at a range of ABP concentrations (2−50 μM), each performed in a series of incubation time (0−160 min). Calculation of the observed inhibition rate constant (k_{obs}) at each ABP concentration (**Fig. 6.10B**) and the subsequent plotting of the k_{obs} values at each ABP concentration (**Fig. 6.10C**) led to a K_I (9.92 μM) and k_{inact} (0.023 min^{-1}) (**Fig. 6.10D**). The calculated pseudo first-order inhibition rate constant (k_{inact} / K_I) is 0.0023 μM^{-1} min^{-1} (**Fig. 6.10D**), which is 10^{-4} times lower than the values for the Cy5 ABP for β- glucuronidase but 1 order higher than the Cy5 ABP for α-iduronidase. The K_I (9.92 μM) was 100-times lower than the K_M of the substrate 4-MU-β-man (0.91 mM)[54], suggesting that ABP **12** has a much higher affinity than the fluorogenic substrate.

6.2.5 Target detection and identification of the β-mannose configured ABPs in mouse kidney homogenates

Chemical proteomics was firstly employed for target identification for the β-mannose configured biotin ABP **13** in mouse kidney extracts, a tissue that is high in MANBA mRNA expression (according to BioGPS dataset GeneAtlas MOE430[56]). The experiment was performed with or without 1 h pre-incubation with 5 μM ABP **11** (BODIPY green). A negative control was also included in which DMSO replaced the ABPs. Analysis of the identified proteins showed that the β-mannosidase MANBA was the only glycosidase identified in samples incubated with ABP **13**, while no glycosidases were detected in the DMSO sample (**Table 6.3**). The sample with ABP **11** pre-incubation showed a reduced PLGS (ProteinLynx Global Server) score and a reduced number of total identified peptide assigned to MANBA, indicating that ABP **11** partially blocked the labeling of the biotin ABP **13** towards MANBA at the tested incubation condition (5 μM, 1 h).

Table 6.3. List of identified glycosidases by LC-MS-based proteomics in samples of mouse kidney extracts incubated with ABP 13. PLGS, ProteinLynx Global Server.

Sample	Accession	Entry	PLGS Score	Peptides	Theoretical peptides	Coverage (%)
# 1 (ABP **13**)	Q8K2I4	MANBA_MOUSE	2825	32	72	33
# 2 (ABP **11** → ABP **13**)	Q8K2I4	MANBA_MOUSE	733	18	72	22
# 3 (DMSO)	N/A	N/A	N/A	N/A	N/A	N/A

Next, the Cy5 ABP **12** was incubated with mouse kidney extracts and followed by SDS-PAGE-based fluorescence detection, to test if MANBA can be specifically visualized. Various ABP concentration (pH 5.5, 2 h), incubation time (pH 5.5, 3 µM), and pH (3 µM, 2 h) were tested. The results showed a distinct band at just below 100 kDa, that was visible at over 1 µM **12** (**Fig. 6.11A**), over 10 min incubation (**Fig. 6.11B**), and between pH 4.5 to 6.0 (optimally at pH 5.0 and 5.5) (**Fig. 6.11C**). The labeling did not saturate in intensity at 10 µM ABP and 120 min incubation, consistent with the labeling and inhibitory potency results with the *Helix pomatia*

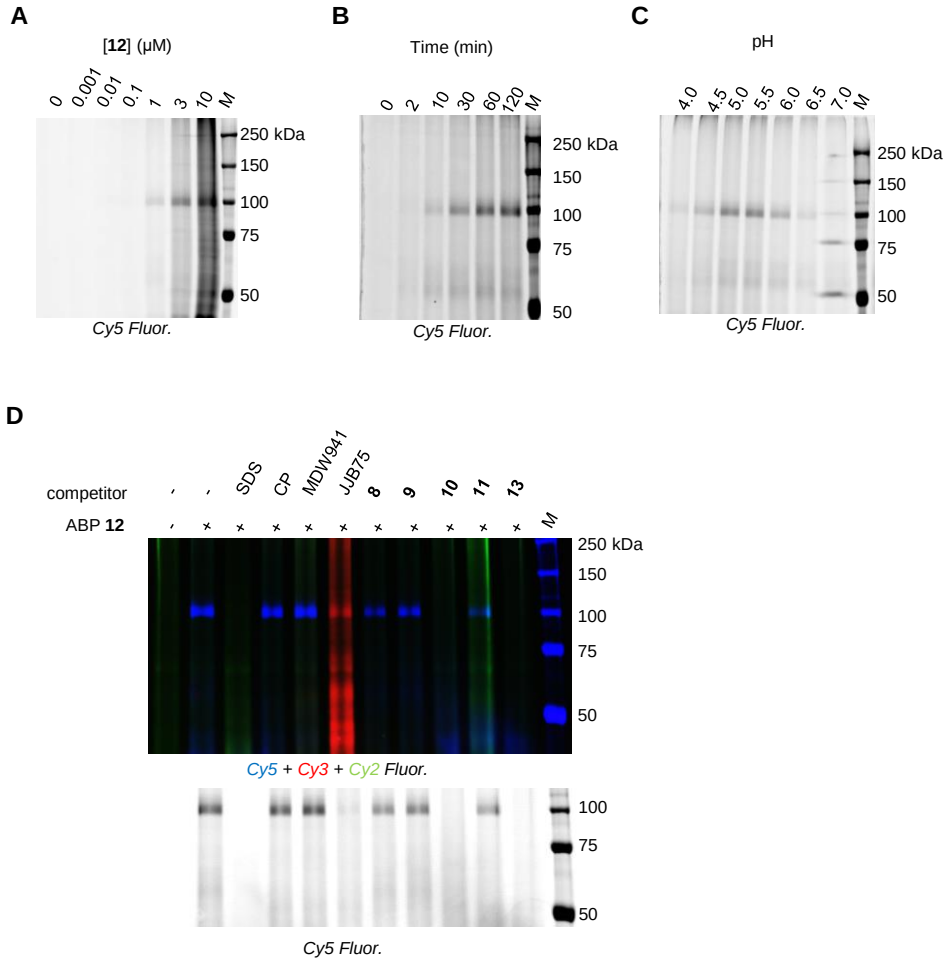

Figure 6.11. cABPP in mouse kidney homogenates. Samples were pre-incubated with competitors or SDS, followed by incubation with ABP **12**. CP, cyclophellitol. JJB75, cyclophellitol aziridine BODIPY-red ABP labeling retaining β-glucosidases.[52, 58]

GH2 β-mannosidase. In addition to the ~100 kDa band, a minor band at ~55 kDa was also noted in the gels. To further verify the identity of both bands, a cABPP experiment was conducted in which mouse kidney extracts were pre-incubated with inhibitors of glucocerebrosidase (GBA, which has a molecular weight of around 55 kDa), retaining β-glucosidases (including GBA2, that has a molecular weight at around 100 kDa), and compounds **8**−**11** and **13**, followed by ABP **12** incubation. The upper band was not abolished by pre-incubation with the GBA and GBA2 inhibitor cyclophellitol (CP, Chapter 2, this thesis) as well as the GBA-specific ABP MDW941[57], and only marginally reduced by compound **8**, **9**, **11**; it was abolished by pre-incubation with the retaining β-glucosidase ABP JJB75[52, 58], compound **10** and **13**, and SDS (**Fig. 6.11**). The labeling on the lower band was not intense enough in this experiment, but cABPP experiment and activity measurements in HEK293T lysates and recombinant enzymes revealed that GBA and GBA2 were both labeled by **12** (**Fig. 6.S5**). Together, these results suggest that the ~100 kDa band in mouse kidney homogenate was likely MANBA. Specific visualization of MANBA was obtainable in samples relatively abundant in MANBA and low in GBA and GBA2, or with pre-incubation with GBA and GBA2 inhibitor.

6.3 Discussion

This chapter describes the characterization of α- and β-mannose configured cyclophellitol aziridine ABPs' activities towards the GH38 α-mannosidases and GH2 β-mannosidase. Both enzyme families are retaining exo-glycosidases, and are involved in metabolism within the protein N-linked glycan pathways. Continuous interest is placed on a number of these enzymes in relation to diseases such as cancer and lysosomal storage disorders. As such, tools to visualize and profile the activity of each of these enzymes would be of great value in laboratory and clinical studies.

The α-mannose configured cyclophellitol and cyclophellitol aziridine compounds (except for the green BODIPY ABP **4**), are low micromolar inhibitors towards the Jack bean (*Canavalis ensiformis*) GH38 α-mannosidase. The alkyl Cy5 ABP **5**'s inhibitory potency increases with prolonged incubation time, and it labels the enzyme in a pH-, concentration-, and time-dependent manner. Its labeling of the enzyme is abolished by pre-incubation of swainsonine and mannostatin A, both known inhibitors of GH38 enzyme. These results suggest the ABP is a mechanism-based irreversible inhibitor of GH38 α-mannosidases. This conclusion is further

substantiated by structural analysis of the *Drosophila* GH38 enzyme dGMII in complex with compound **2**, which shows a glycosidic linkage between the anomeric carbon of the compound and the enzymes catalytic nucleophile, and that the compound adopts the $^{1}S_{5}$ conformation—identical to the one adopted by the enzyme's natural substrates. By gel-based fluorescent ABPP and chemical proteomics, it is shown that the ABPs offer in-class labeling of all five of the GH38 α-mannosidases in mouse tissue extracts, and in HEK293T cells expressing each of the cloned human GH38 enzymes. By tuning the labeling pH, individual mannosidases can be simultaneously profiled on gel in one experiment. The human MAN2B1 is optimally labeled at pH 4.0 to 5.5, and has multiple molecular weight forms (130 kDa, 65 kDa, 45 kDa, 30 kDa) which is likely a result of its complex lysosomal processing.[23, 32] The human MAN2B2 is processed from 130 kDa to 50 kDa. The 50 kDa form was not reported from previous literatures, which all isolated the enzyme in culture medium or tissue fluid instead of from homogenates of cells or whole tissue. Here, it is shown that this 50 kDa form has a pH profile similar to MAN2B1, and is ubiquitously expressed in all mouse tissue tested, as well as in HEK293T cell. Therefore, it is likely that this 50 kDa form of MAN2B2 is the mature lysosomal form, and conveniently, it can be readily distinguished from MAN2B1 based on an ABPP gel based on molecular weight—the first assay that offers simultaneous activity readout of the two enzymes in complex samples. The ABPP assay further identifies endogenous MAN2C1 in mouse brain extracts, which has a molecular weight of around 100 kDa and a pH range between 5.0 to 7.5 (optimally at pH 6.5). It also identifies endogenous MAN2A1 and MAN2A2 in mouse testis and possibly liver extracts, but due to their similar molecular weight it is not possible to discriminate between the two. The best ABP concentration for labeling is 3 μM, as higher concentrations results in more aspecific labeling that complicates interpretation of the results.

The ability of the α-mannose configured ABPs to label all five GH38 α-mannosidases invites two major applications. One would be gel-based fluorescent activity profiling for individual retaining exo-mannosidases across different sample types, to study the processing and activity of these enzymes in different cell/tissue types and in healthy vs. disease context. For example, it could be used to study MAN2C1's involvement in various cancer samples, or be used to monitor the bio-distribution and processing of therapeutic MAN2B1 (or MAN2B1 induced by other potential therapies) in α-mannosidosis patients. Another application is the screening for inhibitors/activators that are specific towards one of the five GH38 enzymes. For example, specific inhibitors for MAN2A1 would offer valuable leads for treating a number of cancers, a

research direction that has been actively pursued.[59, 60] Chaperone/activators for MAN2B1, on the other hand, could lead to alternative therapies for α-mannosidosis. A setup involving fluorescence polarization (FluoPol) ABPP coupled to automated high-throughput screening is currently being investigated (Daniel Lahav, ongoing investigation).

The N-alkylated β-mannose configured cyclophellitol and cyclophellitol aziridine compounds also inhibit their target enzyme—GH2 β-mannosidase—at low micromolar range. The bare cyclophellitol **9** and bare cyclophellitol aziridine **10**, surprisingly, did not inhibit the GH2 β-mannosidase. On the other hand, the Cy5 ABP **12** labels the commercial GH2 enzyme from *Helix pomatia* in a mechanism-based manner., It is noted that the ABP does not avidly label the enzyme between pH 4.0 to 5.0, in contrast to activity measurement using the fluorogenic substrates. As both the enzyme (at 0.1 % (w/v) BSA) and the ABP are stable at this pH range, this noted difference might reflect the intrinsic difference of the enzyme in its reactivity towards the two types of artificial compounds under low pH. Proteomics with the biotin ABP **13** in mouse kidney extracts identified the mouse GH2 enzyme MANBA as the only glycosidase targets. ABPP with the Cy5 ABP **12** in mouse kidney homogenates confirmed that MANBA (around 96 kDa) is labeled, while ABPP in other sample types revealed that the β-glucosidases GBA and GBA2 are also targeted. Interestingly, MANBA in mouse kidney is also labeled by the β-glucose configured cyclophellitol aziridine ABP at the experimental condition (200 nM, 2 h incubation). Despite this, by pre-incubation of specific β-glucosidase inhibitors such as cyclophellitol, MANBA can still be selectively visualized over the β-glucosidases. Next, a novel experimental protocol for determining inhibition kinetic parameters for irreversible inhibitors has also been setup, which is relatively free of substrate during inhibitor incubation and thus should offer a better estimate of inhibition kinetic parameters when compare to the commonly used continuous methods. Application of the β-mannose configured ABPs might not be only restricted to the study in the rare lysosomal storage disorder β-mannosidosis. For instance, it could also be applied in studying other human diseases with abnormal MANBA activity, such as kidney disease.[61]

In conclusion, the presented study in this chapter established that the mannose configured cyclophellitol aziridine ABPs are valuable tools to profile individual retaining exo-mannosidases in complex biological samples. They invite future application in laboratory and clinical investigation of these enzymes in both health and disease.

6.4 Experimental procedures

6.4.1 General materials and methods

All chemicals and reagents were purchased from Sigma Aldrich, if not otherwise stated. HEK293T cells were purchased from ATCC and handled according to the published methods.[62] GH38 α-mannosidase from Jack bean (*Canavalia ensiformis*) and GH2 β-mannosidase from Roman snail (*Helix pomatia*) were purchased from Sigma Aldrich; recombinant GH38 α-mannosidase from *Drosophila melanogaster* (dGMII) was generated according to the methods described in the Appendix section **6.S2.1** and **6.S2.2**. Protein concentration in samples was determined using the Pierce™ BCA kit from Thermo Fisher; for the commercial enzymes, the enzyme stocks were firstly desalted using Pierce™ 7k polyacrylamide desalting spin column (Thermo Fisher) before subjecting to BCA assay; protein concentrations was 1.45 μg (13 pmol) μL^{-1} for *C. e.* α-mannosidase and 2.41 μg (25.6 pmol) μL^{-1} for *H. p.* β-mannosidase. DMSO concentration in samples was kept at 0.5 to 1 % (v/v) during inhibitor/ABP incubation. Coomassie stain were carried out as loading control for SDS-PAGE experiments. HEK293T cells (ATCC CRL-3216) were cultured in DMEM high glucose (Sigma-Aldrich) supplemented with 10 % FCS, 100 units/mL penicillin/streptomycin, and 1 mM Glutamax at 37 °C and at 7 % CO_2.

6.4.2 IC_{50} determination for compound **1**−**7** towards *Canavalia ensiformis* GH38 α-mannosidase

The enzyme (1.45 ng, or 13 fmol) was equilibrated in 12.5 μL McIlvaine buffer (150 mM citric acid/Na_2HPO_4, pH 4.5) for 5 min on ice, and incubated with 12.5 μL inhibitor dilutions (prepared in McIlvaine buffer) for 30 min at 37 °C in black flat-bottom medium-binding 96-well plates (Greiner) in triplicates. Samples were next incubated with 100 μL of substrate mixture (10 mM 4-methylumbelliferyl (4-MU)-α-D-mannopyranoside (4-MU-α-man) in McIlvaine buffer) for 30 min at 37 °C, or for 0−120 min for compound **5**. Reaction was quenched by adding 200 μL 1M Glycine-NaOH (pH 10.3) to the samples. 4-MU fluorescence was measured in the plates using a LS55 fluorometer (PerkinElmer) at λ_{Ex} = 366 nm and λ_{Em} = 445 nm. Measured values were subtracted with background (no enzyme) values, normalized against control values (no inhibitor, with enzyme), and plotted against inhibitor concentrations. IC_{50} values were calculated with Prism 7.0 (GraphPad), using one-phase-exponential decay function. Standard deviations were obtained from 2 sets of calculated IC_{50} values.

6.4.3 Enzymatic activity measurement at various pH

Canavalia ensiformis GH38 α-mannosidase (13 fmol) or *Helix pomatia* GH2 β-mannosidase (340 fmol) were equilibrated in 25 μL McIlvaine buffer for 10 min at 37 °C at various pH (+ 1 mM $ZnCl_2$ for *Canavalia ensiformis* GH38 α-mannosidase), followed by 30 min incubation with 100 μL substrate mixtures (10 mM 4-MU-α-D-mannosylpyranoside (Glycosynth) or 2 mM 4-methylumbelliferyl (4-MU)-β-D-mannosylpyranoside (Glycosynth), 0.1 % (w/v) BSA) at 37 °C. After quenching the reaction by adding 200 μL stop buffer, fluorescence from samples were detected and quantified following methods in a previous section (**6.4.2**).

6.4.4 ABPP with *Canavalia ensiformis* GH38 α-mannosidase

13 fmol of enzyme was equilibrated in 10 μL McIlvaine buffer (+ 1 mM $ZnCl_2$; pH 5.5 if not otherwise indicated) for 5 min on ice, and incubated with ABP **5** (3 μM during incubation, if not otherwise indicated) or ABP **7** (0.1−10 μM during incubation) for 30 min (if not otherwise indicated) at 37 °C. For cABPP experiment, same enzyme dilution was pre-incubated with swainsonine (Cayman Chemical) or mannostatin A (Santa Cruz) at 0.01−3,000 μM for 30 min at 37 °C, followed by ABP **5** incubation (3 μM) for 10 min at 37 °C. After ABP incubation, proteins were denatured and separated by SDS-PAGE, detected and analysed according to the previously described methods.[62, 63]

6.4.5 ABPP with ABP **5** in mouse tissue extracts

Mouse tissue extracts were generated by homogenizing mouse testis sample in four to five volumes of KPi buffer (25 mM K_2HPO_4 / KH_2PO_4, pH 6.5, 0.1 % (v/v) Triton X-100, Protease inhibitor cocktail (EDTA-free, Roche)) in a 2.0 mL screw-cap Eppendorf tube, using 1mm sterile glass beads and FastPrep 24 homogenizer (MP Biomedicals) at 6 m s^{-1} rpm for 20 sec for 3 times. The homogenates were centrifuged at 16,000 rpm for 10 min at 4 °C, and the supernatant was collected and measured for protein concentration using BCA method. Samples were stored in aliquots at −20 °C. For ABPP, samples (40 μg protein) were diluted in 10 μL McIlvaine buffer (150 mM, pH 5.5, if not otherwise stated) and incubated with 5 μL ABP **5** (diluted in McIlvaine buffer) to a final ABP concentration of 3 μM (if not otherwise stated) for 30 min at 37 °C. For competitive ABPP, mouse testis extracts (40 μg protein) were diluted in 10 μL McIlvaine buffer (pH 5.5) and pre-incubated with 0−1,000 μM swainsonine or mannostatin

A in 12.5 µL volume for 30 min at 37 °C, followed by ABP **5** incubation (3 µM) in 15 µL volume for 10 min at 37 °C. Samples were denatured and analyzed by gel-based fluorescent ABPP as described previously.

6.4.6 Proteomics

For pull-down with ABP **6**, 2.5 mg protein from mouse testis extracts were diluted with McIlvaine buffer (750 mM, pH 4.5 or 6.0) to a total volume of 500 µL, and incubated with 10 µM ABP **6** at 37 °C for 1 h. For control, DMSO was used in place of ABP. For pull-down with ABP **13**, 4.0 mg total protein from the kidney extracts were diluted with McIlvaine buffer (750 mM, pH 5.5) in a total volume of 500 µL, and incubated with 10 µM ABP **13** at 37 °C for 1 h, with or without prior pre-incubation with 5 µM ABP **11**. After ABP incubation, samples were denatured with SDS, subjected to chloroform/methanol precipitation (C/M), reduction/alkylation, C/M again, and pull-down with 200 µL streptavidin beads in a volume of 10.2 mL pull-down buffer for O/N at 4 °C following the previously described procedures.[64] Afterwards, half of the samples were subjected to on-bead digestion, and half to in-gel digestion, and desalted using stage-tips according to the described procedures.[64] For LC/MS analysis, 1 µL of sample was injected with phase A (0.1 % (v/v) formic acid in MilliQ H_2O) on a C18 column (Acquity UPLC M-Class 300 µm x 50 mm, packed with BEH C18 material of 1.7 µm diameter and 300 Å pore size particles), eluted with a 50 min gradient of 10 % to 60 % phase B (0.1 % (v/v) formic acid in ACN), followed by 10 min equilibration to 1% phase B at a flow of 0.4 µL/min, hyphenated with Electro-spray ionization (ESI) via Nano-spray source with ESI emitters (New Objectives) fused silica tubing 360 µm OD x 25 µm ID tapered to 5 ± 0.5 µm (5 nL/cm void volume) to a Synapt G2Si mass spectrometer (Waters) operating with Masslynx for acquisition and Ent3 software for polymer envelope signal deconvolution. The following settings in positive resolution mode were used: source temperature of 80 °C, capillary voltage 4.5 kV, nano flow gas of 0.25 Bar, purge gas 250 L/h, trap gas flow 2.0 ml/min, cone gas 100 L/h, sampling cone 25V, source offset 25, trap CE 32V, scan time 3.0 sec, mass range 400-2400 m/z. Lock mass acquiring was done with a mixture of Leu Enk (556.2771) and Glu Fib (785.84265), lockspray voltage 3.5 kV, Glufib fragmentation was used as calibrant. The PLGS (Waters) program was used for data analysis, protein ID or extraction of mgf files for further Mascot (Matrix Science) search analysis. The identification results were exported as Excel file including protein accession numbers, mass of the protein, pI, PLGS score, and % coverage of the protein

by amino acids identified by LC/MS.

6.4.7 Cloning and transient expression of human GH38 α-mannosidases in HEK203T cells

The coding sequences from human GH38 α-mannosidases were PCR-amplified from total cDNA's from human Gaucher spleen using primers listed in **Table 6.S1**. Primers were designed based on NCBI reference sequence NM_002372.3 (MAN2A1), NM_001320977.1 (MAN2A2), NM_000528.4 (MAN2B1), NM_001292038.1 (MAN2B2), and NM_006715.4 (MAN2C1), and cloned into pDNOR-221 and subcloned into pcDNA3.1/Zeo using the Gateway system (Invitrogen). Correctness of the construct was verified by sequencing. Sub-confluent HEK293T cells were transfected with the generated plasmids (or vector plasmids) by the PEI method with a plasmid:PEI ratio 1:3. Media was refreshed 24 h later, and 72 h after transfection, cells were washed three times with phosphate buffered saline (PBS) buffer and collected in KPi buffer. The cell suspension was incubated on ice for 30 min, and stored at −80 °C.

6.4.8 ABPP in lysates of cells expressing the cloned GH38 α-mannosidases

Lysates (20 μg protein) were diluted in 10 μL McIlvaine buffer (150 mM, pH 3.5−7.5, 1 mM $ZnCl_2$), and incubated with 5 μL ABP **5** (diluted in DMSO and 150 mM McIlvaine buffer pH 3.5−7.5, 1 mM $ZnCl_2$) at a final ABP concentration of 3 μM for 30 min at 37 °C. Samples were denatured and analyzed by gel-based fluorescent ABPP as described previously.

6.4.9 Stability test for *Helix pomatia* GH2 β-mannosidase

For the effect of supplements, 340 pmol enzyme was diluted in 25 μL McIlvaine buffer (150 mM) with or without BSA (0.1 % (w/v)), Triton X-100 (0.1 % (v/v)), sodium taurocholate (0.2 % (w/v)), or the combinations of these for 0−120 min at pH 5.5, before subjecting to enzymatic assay (with 100 μL 2 mM 4-MU-β-D-mannopyranoside, 30 min incubation at 37 ºC, pH 5.5, 0.1 % (w/v) BSA). For the effect of pH, same enzyme dilutions were prepared in McIlvaine buffer (+ 0.1 % (w/v) BSA) at various pH values, and incubated for 0−60 min at 37 ºC. Samples were next subjected to the substrate assay (prepared with McIlvaine buffer at matching pH) before activity readout.

6.4.10 ABPP with *Helix pomatia* GH2 β-mannosidase

7.3−51.2 pmol of enzyme was equilibrated in 10 μL McIlvaine buffer (+ 0.1 % w/v BSA, pH

5.5, if not otherwise indicated) for 5 min on ice, and incubated with ABP **12** (3 μM during incubation, if not otherwise indicated) for 30 min (if not otherwise indicated) at 37 °C. After ABP incubation, samples were subjected to SDS-PAGE-based fluorescence detection followed the previously described methods.[62, 63]

6.4.11 IC_{50} determination for compound **8**−**13** towards *Helix pomatia* GH2 β-mannosidase

The enzyme (32.2 ng, or 340 fmol) was equilibrated in 12.5 μL McIlvaine buffer (150 mM, pH 5.5, + 0.1 % v/v Triton X-100) for 5 min on ice, and incubated firstly with the compounds (12.5 μL) for 2 h at 37 °C and secondly with substrates (2 mM 4-MU-β-man) for 1 h at 37 °C. Fluorescence detection and data analysis followed the procedures described in a previous section (**6.4.2**).

6.4.12 Determination of kinetic parameters of ABP **12** towards *helix pomatia* GH2 β-mannosidase

0.9 μg (9.6 pmole) of the enzyme was equilibrated in 120 μL McIlvaine buffer pH 5.5 (150mM, 0.1% (v/v) Triton X-100) and pre-warmed to 37°C for 10 min. For inhibitor incubation, enzymes were combined with equal volume of pre-warmed ABP (prepared in McIlvaine buffer) at 2−50 μM ABP concentrations during incubation, and incubated on a thermoshaker at 37°C. Thereafter, 30 μL aliquots were taken at different time points (0−160 min) from each sample, and subjected to free-ABP removal using polyacrylamide desalting spin column (Pierce). The eluent were diluted 8x with McIlvaine buffer pH 4.5 (150 mM, 0.1% (v/v) Triton-X100), and loaded onto a 96-well plate in 25 μL triplicates. For substrate incubation, 100 μL of pre-warmed substrate mixture (2mM 4-MU-β-D-mannosylpyranoside , dissolved in 150 mM McIlvaine buffer pH 4.5 + 0.1% (v/v) Triton X-100) was added to the samples, and allowed incubation at 37°C for 1 h before subsequent activity measurement. The measured activity was converted to $-\mathrm{Ln}(v_t/v_0)$, with v_t being the rate of substrate hydrolysis at the given time point for a given ABP concentration, and v_0 being the rate at the given time point without ABP incubation. k_{obs} was next determined from the $-\log(V_t/V_0)$ *vs* time plot, using linear regression (GraphPad Prism 7.0). The subsequent k_{obs} *vs* [ABP **12**] plot was used to determine k_{inact} and K_I for ABP **12** towards the enzyme, using the Michaelis-Menten curve-fitting (GraphPad Prism 7.0). For fluorescent gel-based assessment in enzyme yield and free ABP removal, 153.6 pmol enzyme was diluted in 90 μL McIlvaine buffer pH 5.5, and this was incubated with 40 μL ABP 12 for 2 h at 37 ºC, at a

final ABP concentration of 10 μM or 1 μM. Thereafter, 100 μL from each sample was desalted using the spin column, and 90 μL from the eluate was desalted again. Next, 10 μL from the eluates (desalted once or twice) and the un-desalted sample were diluted with 140 μL McIlvaine buffer pH 5.5, and 15 μL from these were loaded onto 10 % polyacrylamide gels for SDS-PAGE and fluorescence detection. The electrophoresis was stopped when the dye front has migrated to about 1 cm from the bottom of the gel.

6.4.13 ABPP using ABP **12** in mouse kidney extracts

25 μg total protein from mouse kidney extracts was diluted in McIlvaine buffer (150 mM, pH 5.5, if not otherwise stated) in a total volume of 10 μL, and incubated with 5 μL ABP **12** (diluted in DMSO and McIlvaine buffer) at final ABP concentration of 3 μM (if not otherwise stated) for 2 h (if not otherwise stated) at 37 °C. cABPP was performed with pre-incubating the extracts with SDS (2 % (w/v)), cyclophellitol (3 μM), ABP MDW941[57] (3 μM), ABP JJB75[52, 58] (3 μM), and compound **8**−**9** (50 μM), **10** (50 μM), **11** (3 μM), and **13** (50 μM) in a volume of 12.5 μL for 2 h at 37 °C, followed by ABP **12** incubation (3 μM) in a volume of 15 μL for 2 h at 37 °C. Samples were denatured and analyzed by gel-based fluorescent ABPP as described previously.

6.4.13 ABPP using ABP **12** in lysates of GBA2-overexpressing HEK293T cells

18.9 μg of lysates from GBA2-overexpressing HEK293T cells (Chapter 2)[62] were pre-incubated with 1 μM of cyclophellitol, the cyclophellitol aziridine BODIPY-red ABP JJB75, compound **8**, **10**, **11**, **13**, or 2 % (w/v) SDS (with 5 min boiling at 98 ºC when pre-incubation completed) at pH 5.5 for 1 h at 37 ºC, and next incubated with 1 μM ABP **12** at pH 5.5 for 2 h at 37 ºC. Samples were denatured and subjected to SDS-PAGE and fluorescence detection. The gel was stained with Coomassie Brilliant Blue G250 for assessing total protein loading amount.

6.4.14 Apparent IC_{50} values of ABP **12** towards recombinant GBA or GBA2

Assays were performed with recombinant GBA, or GBA2 from lysates of overexpressing HEK293T cells using ABP **12** according to the described methods in Chapter 2.[62]

6.5 References

1 Stanley P, Taniguchi N & Aebi M (2017) N-Glycans. In Varki A, Cummings RD, Esko JD, Stanley P, Hart GW, Aebi M, Darvill AG, Kinoshita T, Packer NH, Prestegard JH, Schnaar RL & Seeberger PH (Eds) *Essentials of Glycobiology [Internet]. 3rd edition*. Cold Spring Harbor, NY: Cold Spring Harbor Laboratory Press.

2 Schwarz F & Aebi M (2011) Mechanisms and principles of N-linked protein glycosylation. *Curr Opin Struct Biol* **21**, 576–582.

3 Lombard V, Golaconda Ramulu H, Drula E, Coutinho PM & Henrissat B (2014) The Carbohydrate-active enzymes database (CAZy) in 2013. *Nucleic Acids Res* **42**, D490–D495.

4 Avezov E, Frenkel Z, Ehrlich M, Herscovics A & Lederkremer GZ (2008) Endoplasmic reticulum (ER) mannosidase I is compartmentalized and required for N-glycan trimming to Man5-6GlcNAc2 in glycoprotein ER-associated degradation. *Mol Biol Cell* **19**, 216–225.

5 Wu Y, Swulius MT, Moremen KW & Sifers RN (2003) Elucidation of the molecular logic by which misfolded alpha 1-antitrypsin is preferentially selected for degradation. *Proc Natl Acad Sci USA* **100**, 8229–8234.

6 Helenius A & Aebi M (2004) Roles of N-linked glycans in the endoplasmic reticulum. *Annu Rev Biochem* **73**, 1019–1049.

7 Słomińska-Wojewódzka M & Sandvig K (2015) The Role of Lectin-Carbohydrate Interactions in the Regulation of ER-Associated Protein Degradation. *Molecules* **20**, 9816—9846.

8 Lal A, Schutzbach JS, Forsee WT, Neame PJ & Moremen KW (1994) Isolation and expression of murine and rabbit cDNAs encoding an alpha 1,2-mannosidase involved in the processing of asparagine-linked oligosaccharides. *J Biol Chem* **269**, 9872–9881.

9 Herscovics A, Schneikert J, Athanassiadis A & Moremen KW (1994) Isolation of a mouse Golgi mannosidase cDNA, a member of a gene family conserved from yeast to mammals. *J Biol Chem* **269**, 9864–9871.

10 Tremblay LO & Herscovics A (2000) Characterization of a cDNA encoding a novel human Golgi alpha 1, 2-mannosidase (IC) involved in N-glycan biosynthesis. *J Biol Chem* **275**, 31655–31660.

11 Braulke T & Bonifacino JS (2009) Sorting of lysosomal proteins. *Biochim Biophys Acta* **1793**, 605–614.

12 Lubas WA & Spiro RG (1987) Golgi endo-alpha-D-mannosidase from rat liver, a novel N-linked carbohydrate unit processing enzyme. *J Biol Chem* **262**, 3775–3781.

13 Lubas WA & Spiro RG (1988) Evaluation of the role of rat liver Golgi endo-alpha-D-mannosidase in processing N-linked oligosaccharides. *J Biol Chem* **263**, 3990–3998.

14 Moremen KW & Robbins PW (1991) Isolation, characterization, and expression of cDNAs encoding murine alpha-mannosidase II, a Golgi enzyme that controls conversion of high mannose to complex N-glycans. *J Cell Biol* **115**, 1521–1534.

15 Misago M, Liao YF, Kudo S, Eto S, Mattei MG, Moremen KW & Fukuda MN (1995) Molecular cloning and expression of cDNAs encoding human alpha-mannosidase II and a previously unrecognized alpha-mannosidase IIx isozyme. *Proc Natl Acad Sci USA* **92**, 11766–11770.

16 Shah N, Kuntz DA & Rose DR (2008) Golgi alpha-mannosidase II cleaves two sugars sequentially in the same catalytic site. *Proc Natl Acad Sci USA* **105**, 9570–9575.

17 Akama TO, Nakagawa H, Wong NK, Sutton-Smith M, Dell A, Morris HR, Nakayama J, Nishimura S, Pai A, Moremen KW, Marth JD & Fukuda MN (2006) Essential and mutually compensatory roles of alpha-mannosidase II and alpha-mannosidase IIx in N-glycan processing in vivo in mice. *Proc Natl Acad Sci USA* **103**, 8983–8988.

18 Fukuda MN, Masri KA, Dell A, Luzzatto L & Moremen KW (1990) Incomplete synthesis of N-glycans in congenital dyserythropoietic anemia type II caused by a defect in the gene encoding alpha-mannosidase II. *Proc Natl Acad Sci USA* **87**, 7443–7447.

19 Fukuda MN & Akama TO (2002) *In vivo* role of alpha-mannosidase IIx: ineffective spermatogenesis resulting from targeted disruption of the Man2a2 in the mouse. *Biochim Biophys Acta* **1573**, 382–387.

20 Suzuki T, Hara I, Nakano M, Shigeta M, Nakagawa T, Kondo A, Funakoshi Y & Taniguchi N (2006) Man2C1, an alpha-mannosidase, is involved in the trimming of free oligosaccharides in the cytosol. *Biochem J* **400**, 33–41.

21 Suzuki T & Harada Y (2014) Non-lysosomal degradation pathway for N-linked glycans and dolichol-linked

oligosaccharides. *Biochem Biophys Res Commun* **453**, 213–219.

22 Kuokkanen E, Smith W, Mäkinen M, Tuominen H, Puhka M, Jokitalo E, Duvet S, Berg T & Heikinheimo P (2007) Characterization and subcellular localization of human neutral class II alpha-mannosidase [corrected]. *Glycobiology* **17**, 1084–1093.

23 Liao YF, Lal A & Moremen KW (1996) Cloning, expression, purification, and characterization of the human broad specificity lysosomal acid alpha-mannosidase. *J Biol Chem* **271**, 28348–28358.

24 Damme M, Morelle W, Schmidt B, Andersson C, Fogh J, Michalski JC & Lübke T (2010) Impaired lysosomal trimming of N-linked oligosaccharides leads to hyperglycosylation of native lysosomal proteins in mice with alpha-mannosidosis. *Mol Cell Biol* **30**, 273–83.

25 De Gasperi R, Daniel PF & Warren CD (1992) A human lysosomal alpha-mannosidase specific for the core of complex glycans. *J Biol Chem* **267**, 9706–9712.

26 Park C, Meng L, Stanton LH, Collins RE, Mast SW, Yi X, Strachan H & Moremen KW (2005) Characterization of a human core-specific lysosomal alpha 1,6-mannosidase involved in N-glycan catabolism. *J Biol Chem* **280**, 37204–37216.

27 Okamura N, Tamba M, Liao HJ, Onoe S, Sugita Y, Dacheux F & Dacheux JL (1995) Cloning of complementary DNA encoding a 135-kilodalton protein secreted from porcine corpus epididymis and its identification as an epididymis-specific alpha-mannosidase. *Mol Reprod Dev* **42**, 141–148.

28 Alkhayat AH, Kraemer SA, Leipprandt JR, Macek M, Kleijer WJ & Friderici KH (1998) Human beta-mannosidase cDNA characterization and first identification of a mutation associated with human beta-mannosidosis. *Hum Mol Genet* **7**, 75–83.

29 Samra ZQ & Athar MA (2008) Cloning, sequence, expression and characterization of human beta-mannosidase. *Acta Biochim Pol* **55**, 479–490.

30 van den Elsen JM, Kuntz DA & Rose DR (2001) Structure of Golgi alpha-mannosidase II: a target for inhibition of growth and metastasis of cancer cells. *EMBO J* **20**, 3008–3017.

31 Goss PE, Reid CL, Bailey D & Dennis JW (1997) Phase IB clinical trial of the oligosaccharide processing inhibitor swainsonine in patients with advanced malignancies. *Clin Cancer Res* **3**, 1077–1086.

32 Heikinheimo P, Helland R, Leiros HK, Leiros I, Karlsen S, Evjen G, Ravelli R, Schoehn G, Ruigrok R, Tollersrud OK, McSweeney S & Hough E (2003) The structure of bovine lysosomal alpha-mannosidase suggests a novel mechanism for low-pH activation. *J Mol Biol* **327**, 631–44.

33 Malm D & Nilssen Ø (2008) Alpha-mannosidosis. *Orphanet J Rare Dis* **3**, 21.

34 Ceccarini MR, Codini M, Conte C, Patria F, Cataldi S, Bertelli M, Albi E & Beccari T (2018) Alpha-Mannosidosis: Therapeutic Strategies. *Int J Mol Sci* **19**, E1500.

35 Harmatz P, Cattaneo F, Ardigò D, Geraci S, Hennermann JB, Guffon N, Lund A, Hendriksz CJ & Borgwardt L (2018) Enzyme replacement therapy with velmanase alfa (human recombinant alpha-mannosidase): Novel global treatment response model and outcomes in patients with alpha-mannosidosis. *Mol Genet Metab* **124**, 152–160.

36 Bedilu R, Nummy KA, Cooper A, Wevers R, Smeitink J, Kleijer WJ & Friderici KH (2002) Variable clinical presentation of lysosomal beta-mannosidosis in patients with null mutations. *Mol Genet Metab* **77**, 282–290.

37 Jones MZ & Dawson G (1981) Caprine beta-mannosidosis. Inherited deficiency of beta-D-mannosidase. *J Biol Chem* **256**, 5185–5188.

38 Tian Y, Ju JY, Zhou YQ, Liu Y & Zhu LP (2008) Inhibition of alpha-mannosidase Man2c1 gene expression suppresses growth of esophageal carcinoma cells through mitotic arrest and apoptosis. *Cancer Sci* **99**, 2428–2434.

39 Xiang ZG, Jiang DD, Liu Y, Zhang LF & Zhu LP (2010) hMan2c1 transgene promotes tumor progress in mice. *Transgenic Res* **19**, 67–75.

40 He L, Fan C, Kapoor A, Ingram AJ, Rybak AP, Austin RC, Dickhout J, Cutz JC, Scholey J & Tang D (2011) α-Mannosidase 2C1 attenuates PTEN function in prostate cancer cells. *Nat Commun* **2**, 307.

41 Wang L & Suzuki T (2013) Dual functions for cytosolic α-mannosidase (Man2C1): its down-regulation causes mitochondria-dependent apoptosis independently of its α-mannosidase activity. *J Biol Chem* **288**, 11887–11896.

42 Daniel PF, Winchester B & Warren CD (1994) Mammalian alpha-mannosidases—multiple forms but a common purpose? *Glycobiology* **4**, 551–566.

43 Numao S, Kuntz DA, Withers SG & Rose DR (2003) Insights into the mechanism of Drosophila melanogaster

Golgi alpha-mannosidase II through the structural analysis of covalent reaction intermediates. *J Biol Chem* **278**, 48074–48083.

44 Tailford LE, Offen WA, Smith NL, Dumon C, Morland C, Gratien J, Heck MP, Stick RV, Blériot Y, Vasella A, Gilbert HJ & Davies GJ (2008) Structural and biochemical evidence for a boat-like transition state in beta-mannosidases. *Nat Chem Biol* **4**, 306-312.

45 Davies GJ, Planas A, Rovira C (2012) Conformational analyses of the reaction coordinate of glycosidases. *Acc Chem Res* **45**, 308–316.

46 Wong C-S (2015) Chapter 5. In *The synthesis of mannose-derived bioconjugates and enzyme inhibitors* (Doctoral dissertation) (pp 141−116). Retrieved from Leiden University Repository.

47 Ritzen B, van Oers MC, van Delft FL & Rutjes FP (2009) Enantioselective chemoenzymatic synthesis of trans-aziridines. *J Org Chem.* 74, 7548-7551.

48 Beenakker TJM (2018) Chapter 4. In *Design and development of conformational inhibitors and activity-based probes for retaining glycosidases* (Doctoral dissertation) (pp 47−60). Retrieved from Leiden University Repository.

49 Beenakker TJM (2018) Chapter 5. In *Design and development of conformational inhibitors and activity-based probes for retaining glycosidases* (Doctoral dissertation) (pp 61−74). Retrieved from Leiden University Repository.

50 Howard S, Braun C, McCarter J, Moremen KW, Liao YF & Withers SG (1997) Human lysosomal and jack bean alpha-mannosidases are retaining glycosidases. *Biochem Biophys Res Commun* **238**, 896−898.

51 Tatsuta K, Niwata Y, Umezawa K, Toshima K & Nakata M (1991) Syntheses and enzyme inhibiting activities of cyclophellitol analogs. *J Antibiot (Tokyo)* **44**, 912−914.

52 Jiang J, Beenakker TJ, Kallemeijn WW, van der Marel GA, van den Elst H, Codée JD, Aerts JM & Overkleeft HS (2015) Comparing Cyclophellitol N-Alkyl and N-Acyl Cyclophellitol Aziridines as Activity-Based Glycosidase Probes. *Chemistry* **21**, 10861−10869.

53 Howard S, He S & Withers SG (1998) Identification of the active site nucleophile in jack bean alpha-mannosidase using 5-fluoro-beta-L-gulosyl fluoride. *J Biol Chem* **273**, 2067−2072.

54 McCleary BV (1983) beta-D-Mannosidase from Helix pomatia. Carbohydr Res 111, 297−310.

55 Remen L & Vasella A (2002) *Helv Chim Acta* **85**, 1118−1127.

56 Wu C, Jin X, Tsueng G, Afrasiabi C & Su AI (2016) BioGPS: building your own mash-u of gene annotations and expression profiles. *Nucleic Acids Res* **44**(D1), D313−316.

57 Witte MD, Kallemeijn WW, Aten J, Li KY, Strijland A, Donker-Koopman WE, van den Nieuwendijk AM, Bleijlevens B, Kramer G, Florea BI, Hooibrink B, Hollak CE, Ottenhoff R, Boot RG, van der Marel GA, Overkleeft HS & Aerts JM (2010) Ultrasensitive in situ visualization of active glucocerebrosidase molecules. *Nat Chem Biol* **6**, 907−913.

58 Kallemeijn WW, Li KY, Witte MD, Marques AR, Aten J, Scheij S, Jiang J, Willems LI, Voorn-Brouwer TM, van Roomen CP, Ottenhoff R, Boot RG, van den Elst H, Walvoort MT, Florea BI, Codée JD, van der Marel GA, Aerts JM & Overkleeft HS (2012) Novel activity-based probes for broad-spectrum profiling of retaining β-exoglucosidases *in situ* and *in vivo*. *Angew Chem Int Ed Engl* **51**, 12529−12533.

59 Howard E, Cousido-Siah A, Lepage ML, Schneider JP, Bodlenner A, Mitschler A, Meli A, Izzo I, Alvarez HA, Podjarny A & Compain P (2018) Structural basis of outstanding multivalent effects in jack bean α-mannosidase inhibition. *Angew Chem Int Ed Engl* **57**, 8002−8006.

60 Gerber-Lemaire S & Juillerat-Jeanneret L (2010) Studies toward new anti-cancer strategies based on alpha-mannosidase inhibition. *Chimia (Aarau)* **64**, 634−639.

61 Ko YA, Yi H, Qiu C, Huang S, Park J, Ledo N, Köttgen A, Li H, Rader DJ, Pack MA, Brown CD & Susztak K (2017) Genetic-Variation-Driven Gene-expression changes highlight genes with important functions for kidney disease. *Am J Hum Genet* **100**, 940−953.

62 Kuo CL, Kallemeijn WW, Lelieveld LT, Mirzaian M, Zoutendijk I, Vardi A, Futerman AH, Meijer AH, Spaink HP, Overkleeft HS, Aerts JMFG & Artola M (2019) *In vivo* inactivation of glycosidases by conduritol B epoxide and cyclophellitol as revealed by activity-based protein profiling. *FEBS J* **286**, 584−600.

63 Kuo CL, van Meel E, Kytidou K, Kallemeijn WW, Witte M, Overkleeft HS, Artola ME & Aerts JM (2018) Activity-based probes for glycosidases: profiling and other applications. *Methods Enzymol* **598**, 217−235.

64 Li N, Kuo CL, Paniagua G, van den Elst H, Verdoes M, Willems LI, van der Linden WA, Ruben M, van Genderen E, Gubbens J, van Wezel GP, Overkleeft HS & Florea BI (2013) Relative quantification of proteasome activity

by activity-based protein profiling and LC-MS/MS. *Nat Protoc* **8**, 1155−1168.

APPENDIX

6.S1. Supporting Figures and Tables

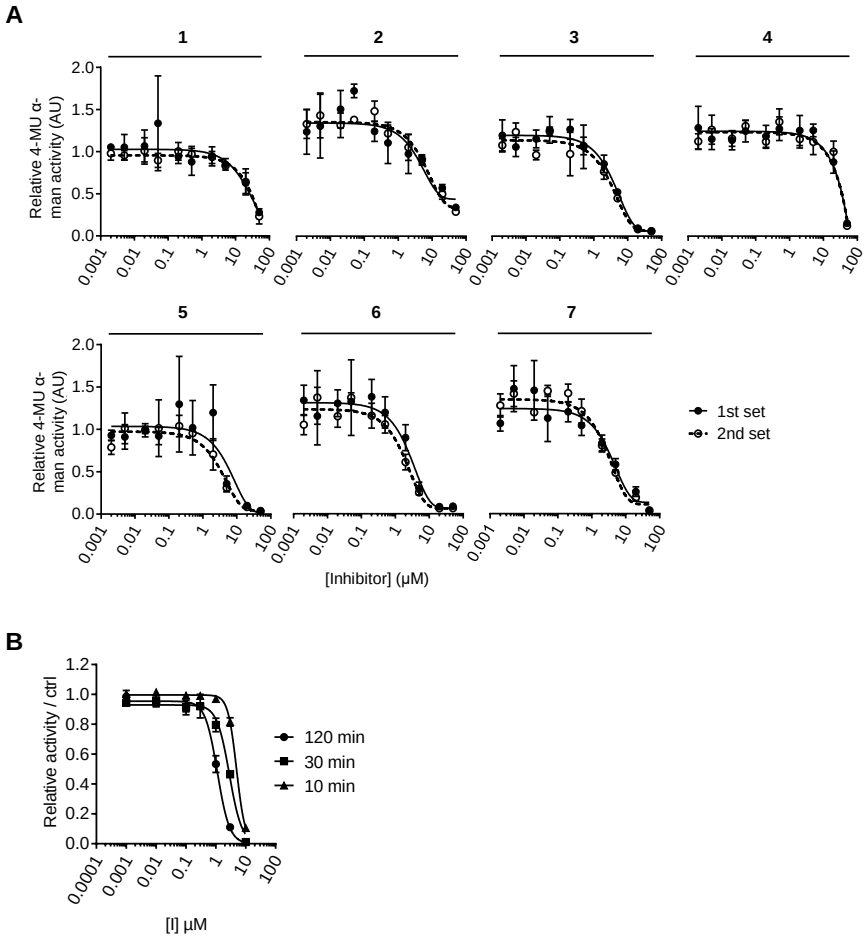

Figure 6.S1. Inhibition curves of compound 1−7 towards Jack bean (*Canavalis ensiformis*) GH38 α-mannosidase for apparent IC_{50} determination. A) 30 min incubation. B) 30−120 min incubation. Error range = ± SD (*n* = 3 technical replicates).

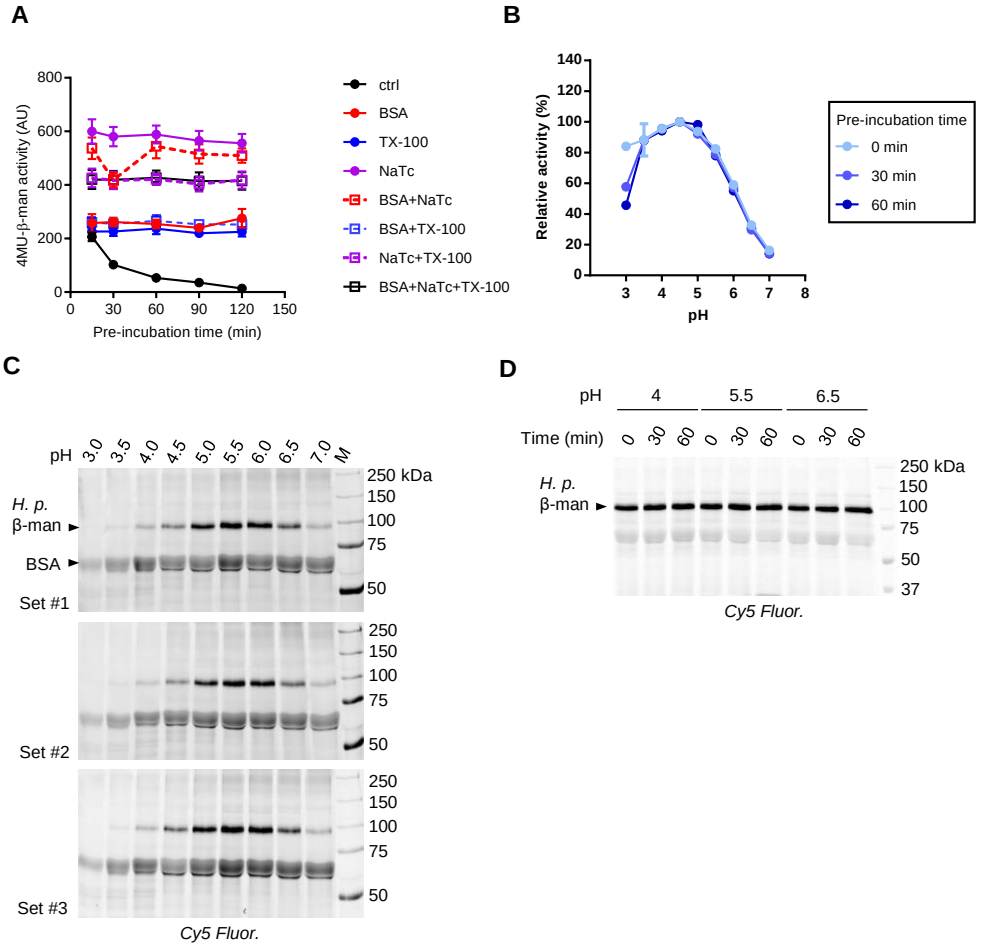

Figure 6.S2. Characterization of ABP labeling conditions for *Helix pomatia* GH2 β-mannosidase. A) Measured enzyme activity (30 min with 4-MU β-man substrate assay at pH 5.5) with or without supplements, over the indicated pre-incubation periods at pH 5.5. B) Effect of pH on enzymatic activity at various pH and over different pre-incubation periods, in the presence of 0.1 % (w/v) BSA. C) ABP **12** labeling at various pH value, in the presence of 0.1 % (w/v) BSA. D) Effect of pre-incubating ABP **12** at pH 4.0, 5.5, and 6.5 for 0, 30, or 60 min at 37 ºC on its labeling towards the enzyme (at 10 µM [ABP], pH 5.5, 1 h 37 ºC). Error range = ± SD (*n* = 3, technical replicates).

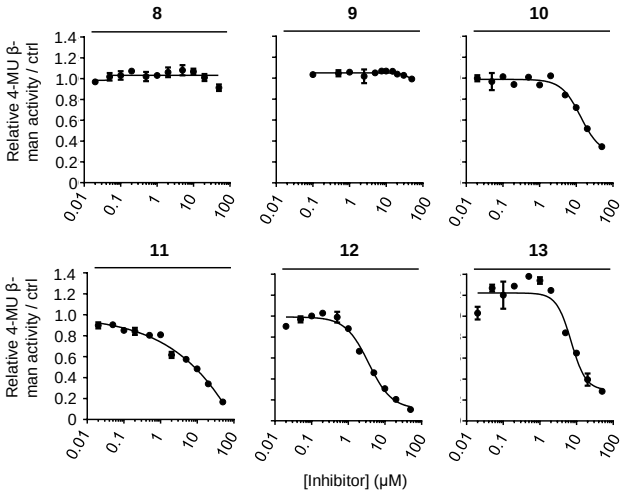

Figure 6.S3. Inhibition curves of compound 8−13 for apparent IC_{50} determination in snail (*Helix pomatia*) GH2 β-mannosidase. Error range = ± SD, *n* = 3 technical replicates.

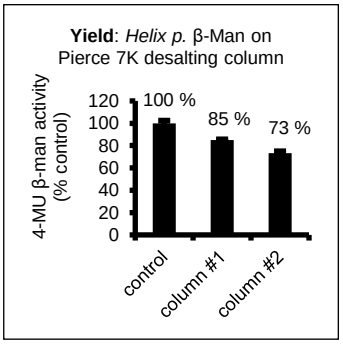

Figure 6.S4. Activity of snail (*Helix pomatia*) GH2 β-mannosidase after desalting. Error range = ± SD, *n* = 3 technical replicates.

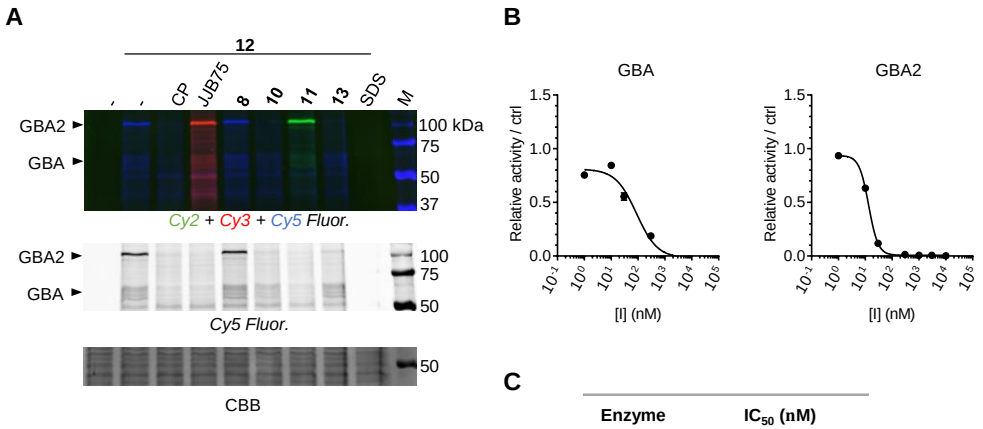

Enzyme	IC_{50} (nM)
GBA	87.8 ± 19.4
GBA2	13.4 ± 0.232

Figure 6.S5. Reactivity of ABP 12 towards retaining β-glucosidases. A) cABPP in lysates of GBA2-overexpressed HEK293T cells, using pre-incubation of cyclophellitol (CP), ABP JJB75, compounds **8**, **10**, **11**, **13**, and 2 % (w/v) SDS. *CBB*, Coomassie Brilliant Blue staining. B) Inhibition curves on GBA, GBA2, and GBA3. C) Apparent IC_{50} values. Error range = ± SD (*n* = 3 technical replicates).

Table 6.S1. Primers used for coning human GH38 α-mannosidases

Protein	Primer	Sequence
MAN2A1	Forward	GGGGACAAGTTTGTACAAAAAAGCAGGCTACCACCATGAAGTTAAGCCGCCAGTTCAC
	Reverse	GGGGACCACTTTGTACAAGAAAGCTGGGTCTCACCTCAACTGGATTCGGAATG
MAN2A2	Forward	GGGGACAAGTTTGTACAAAAAAGCAGGCTACCACCATGAAGCTGAAAAAGCAGGTGAC
	Reverse	GGGGACCACTTTGTACAAGAAAGCTGGGTCCTAACCCAAGCGGAGGCGAAAGG
MAN2B1	Forward	GGGGACAAGTTTGTACAAAAAAGCAGGCTACCACCATGGGCGCCTACGCGCGGGCTTC
	Reverse	GGGGACCACTTTGTACAAGAAAGCTGGGTCCTAACCATCCACCTCCTTCCATTG
MAN2B2	Forward	GGGGACAAGTTTGTACAAAAAAGCAGGCTACCACCATGGGGCAGCTGTGCTGGCTGC
	Reverse	GGGGACCACTTTGTACAAGAAAGCTGGGTCTCACTGCTGTTGAAAGTGAATAA
MAN2C1	Forward	GGGGACAAGTTTGTACAAAAAAGCAGGCTACCACCATGGCGGCTGCGCCGGCCTTG
	Reverse	GGGGACCACTTTGTACAAGAAAGCTGGGTCTCAGTGTGGCGGAGGCTGAAG

6.S2. Supporting experimental procedures for protein X-ray crystallography (University of York)

6.S2.1 Cloning and expression of dGMII

A plasmid containing cDNA encoding for the dGMII gene was obtained with kind permission from Dr. Sean Sweeny (University of York). From this plasmid, cDNA encoding for amino acids 76-1108 of dGMII (to remove the N-terminal cytosolic, transmembrane, and stalk domains) was subcloned into the pOMNIBac vector (Geneva Biotech), behind a honeybee mellitin secretion peptide, 6xHis tag, and TEV cleavage site. Recombinant bacmid was produced using the Tn7 transposition method in DH10EMBacY (Geneva Biotech)[1], and purified using the PureLink miniprep kit (Invitrogen) following standard protocols. V1 baculovirus was produced by transfection of bacmid into low passage adherent Sf21 cells (Invitrogen) using FuGENE HD transfection reagent (ProMega), at a ratio of 2 µg DNA to 4.5 µL FuGENE. V1→V2 virus amplification was carried out using suspension Sf21 cells, using the YFP marker present in EMBacY baculovirus to determine optimum amplification prior to harvesting (typically ~60 % cells fluorescent). For expression, *T. Ni* cells (Invitrogen) were infected with V2 baculovirus at a multiplicity of infection (MOI) > 1, and infection followed using the EMBacY YFP marker to determine optimum timepoint for harvesting (typically 72 h, with > 80 % cells fluorescent). All insect cells used tested negative for mycoplasma contamination.

6.S2.2 Purification of dGMII

Harvested High Five cultures were spun for 15 minutes at 200 g to remove cells and spun again at 4000 g for 1 hour to remove insoluble cellular components. AEBSF (to a final concentration of 0.1 mM) and DDT (to a final concentration of 1 mM) were added to the supernatant. Clarified supernatant was loaded on to 2 x 5mL HiTrap Blue HP columns (GE Healthcare) pre-equilibrated in blue agarose buffer A (20 mM HEPES pH 7.4, 100 mM NaCl, 1 mM DTT). Loaded columns were washed with 5 column volumes of blue agarose buffer A and eluted using a linear gradient of blue agarose buffer B (20 mM HEPES pH 7.4, 2 M NaCl, 1 mM DTT) over 20 column volumes. HiTrap Blue fractions containing dGMII (as determined by SDS-PAGE) were pooled and diluted approximately 5-fold in HisTrap buffer A (50 mM HEPES pH 8.0, 0.5 M NaCl, 30 mM Imidazole, 1 mM DTT) and loaded on to a 1 mL HisTrap FF Crude column (GE Healthcare) The loaded HisTrap column was washed with 10 column volumes of HisTrap

buffer A and dGMII eluted using a linear gradient of HisTrap buffer B (50 mM HEPES pH 8.0, 0.5 M NaCl, 0.5 M imidazole, 1 mM DTT) over 20 column volumes, followed by 10 column volumes of 100 % Buffer B. HisTrap fractions containing dGMII were pooled and concentrated to less than 2 ml by centrifugation using VivaSpin 30,000 MW concentrator (GE Healthcare). Pooled dGMII was rediluted to ~2 mL in 1x AcTEV (Invitrogen) reaction buffer before addition of 5 µL AcTEV protease to remove the N-HisTEV tag. Digests were typically carried out overnight at ambient temperature, and reaction progress assessed by comparison to positive and negative controls using SDS-PAGE. Upon completion of the AcTEV digest, as indicated by SDS-PAGE, dGMII was purified using a S200 16/600 size exclusion chromatography (SEC) column equilibrated in SEC buffer (50 mM HEPES pH 7.4, 200 mM NaCl, 1 mM DTT), at 1 ml min-1. SEC fractions containing dGMII were pooled, concentrated to 10 mg ml-1 and stored in 20 µl aliquots at −80 °C.

6.S2.3 3D Crystallography of dGMII

Initial crystallization conditions were screened using JCSG+ HT-96, PACT premier HT-96 (both Molecular Dimensions), Index HT and PEG/Ion HT (both Hampton Research) commercial screens. Hits were optimized, scaled up to maxi 48-well plates and a dGMII seed stock generated from crystals grown in 0.1 M imidazole pH 7.0 and 10 % (w/v) PEG 3350 using the Seed Bead protocol (Hampton Research). The above screens were repeated with seeding using an Oryx8 (Douglas Instruments) and additional hits optimized further. Diffraction quality dGMII crystals were grown in maxi 48-well plates using sitting drop vapor diffusion in 0.1 M sodium succinate pH 7.0 and 10 % (w/v) PEG 3350. Crystals were cryoprotected using cryoprotectant solution (mother liquor supplemented with 25% v/v ethylene glycol) prior to flash freezing in liquid N_2 for data collection. Dataset collection and processing followed the previous methods.[2] Apo dGMII was solved by molecular replacement with PDB model 1HWW[main text ref 30] using MolRep[3], followed by alternating rounds of manual model building and refinement using Coot and REFMAC5 respectively[4, 5]. For ligand complexes, dGMII crystals were soaked in solutions of **2** (1 mM) in dGMII cryoprotectant solution for ~3 hours before flash freezing in liquid N_2 for data collection. Complexes were solved by molecular replacement with the apo dGMII structure, followed by rounds of manual model building and refinement using Coot and REFMAC5. Generation of crystal structure figures and ligand coordinates followed the described methods.[2]

6.S3. Synthetic strategies for compounds used in this chapter (Department of Bio-organic Synthesis, Leiden University)

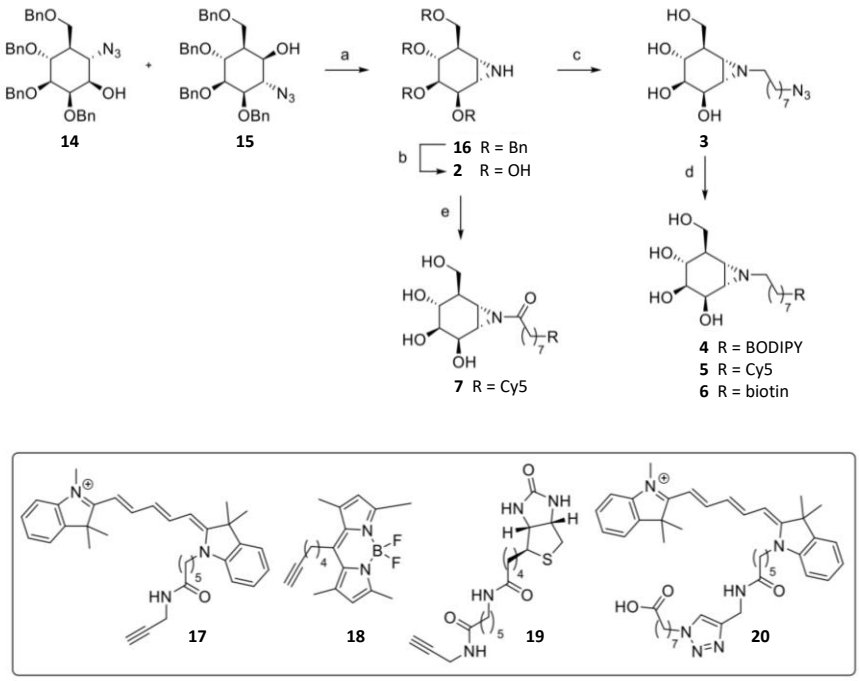

Scheme 6.S1. Synthetic strategy of compound 2−7. Reagents and conditions: a) PPh_3 polymer-bound on styrene-divinylbenzene copolymer, CH_3CN, reflux, overnight, 54 %; b) Li, THF, NH3 (l), −60 °C, 75 min; c) 1-azido-8-iodooctane (see Chapter 6), K_2CO_3, DMF, 80 °C, overnight, 38 % over 2 steps; d) **17**[6], **18**[7] or **19**[8], $Cu.SO_4 \cdot 5H_2O$, sodium ascorbate, DMF, RT, **4** 35 %, **5** 8.5 %, **6** 16 %; e) **20**[6], EEDQ, DMF, 0 °C, 2.5 h, 8 % over 2 steps.

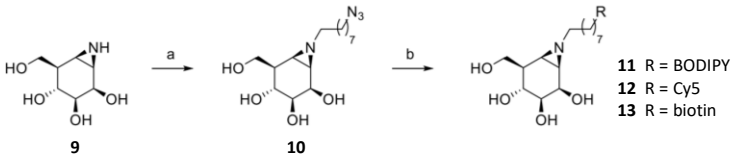

Scheme 6.S2. Synthetic strategy of compound 9−13. Reagents and conditions: a) 1-azido-8-iodooctane (see Chapter 4), K_2CO_3, DMF, 80 °C, overnight, 64 %; b) **17**[6], **18**[7] or **19**[8], $Cu.SO_4 \cdot 5H_2O$, sodium ascorbate, **11** 17 %, 12 36 % and **13** 32 %.

Supporting References

1 Bieniossek C, Imasaki T, Takagi Y & Berger I (2012) MultiBac: expanding the research toolbox for multiprotein complexes. Trends Biochem Sci **37**, 49−57.

2 Wu L, Jiang J, Jin Y, Kallemeijn WW, Kuo CL, Artola M, Dai W, van Elk C, van Eijk M, van der Marel GA, Codée JDC, Florea BI, Aerts JMFG, Overkleeft HS & Davies GJ (2017) Activity-based probes for functional interrogation of retaining β-glucuronidases. *Nat Chem Biol* **13**, 867−873.

3 Vagin A & Teplyakov A (2010) Molecular replacement with MOLREP. *Acta Crystallogr D Biol Crystallogr* **66**(Pt 1), 22−25.

4 Emsley P, Lohkamp B, Scott WG & Cowtan K (2010) Features and development of Coot. *Acta Crystallogr D Biol Crystallogr* **66**(Pt 4), 486−501.

5 Murshudov GN, Skubák P, Lebedev AA, Pannu NS, Steiner RA, Nicholls RA, Winn MD, Long F & Vagin AA (2011) REFMAC5 for the refinement of macromolecular crystal structures. *Acta Crystallogr D Biol Crystallogr* **67**(Pt 4), 355−367.

6 Beenakker TJM (2018) Chapter 2. In *Design and development of conformational inhibitors and activity-based probes for retaining glycosidases* (Doctoral dissertation) (pp 13−27). Retrieved from Leiden University Repository.

7 Verdoes M, Hillaert U, Florea BI, Sae-Heng M, Risseeuw MD, Filippov DV, van der Marel GA & Overkleeft HS (2007) Acetylene functionalized BODIPY dyes and their application in the synthesis of activity based proteasome probes. *Bioorg Med Chem Lett* **17**, 6169−6171.

8 Inoue M, Tong W, Esko JD & Tor Y (2013) Aggregation-mediated macromolecular uptake by a molecular transporter. *ACS Chem Biol* **8**, 1383−1388.